RSC Advances

PAPER

View Article Online
View Journal | View Issue

Cite this: *RSC Adv.*, 2026, **16**, 5374

Design and synthesis of novel sulfa-azo dyes: a sustainable approach to textile dyeing combined with microwave energy

Salma Sherif,[a] Asmaa Aboelnaga,[*a] Nagla S. Elshemy,[b] Samia Elabbady[a] and Sayed K. Ramadan[*c]

As bacteria continue to resist antimicrobial medications, there is a need to develop new compounds. In this work, new sulfonamide-based azo dyes with antimicrobial qualities are synthesized and dyed on fabric using microwave irradiation, an energy-efficient substitute for traditional heating techniques. First, azo linkage was formed at the amine groups of sulfathiazole and sulfamethoxazole, then the diazonium salt coupled with different nucleophilic couplers like 1,3-indandione and 1-indanone. The produced dyes were structurally confirmed using mass, IR, ^{1}H NMR, and ^{13}C NMR spectral data. Molecular docking studies revealed favorable binding affinity toward both *p*ABA- and Pterin-binding amino acid residues, suggesting potential dual DHPS inhibitory behavior. Molecular docking studies of the synthesized sulfa-azo dyes showed encouraging antimicrobial activity. Potential dual inhibitors of DHPS were indicated by the fact that several dyes demonstrated binding with both *p*ABA and Pterin amino acids. Additionally, certain dyes aligned with known co-crystallized inhibitors by interacting with fungal *N*-myristoyltransferase (NMT). The strongest antibacterial activity was shown by dyes made from indandione and indanone couplers. As a contemporary heating technique, microwave irradiation was used to increase reaction efficiency, lower chemical and water usage, and save energy. Through polarization processes such as electronic, atomic, and interfacial polarization, the improved interaction between microwave energy and polar molecules caused rapid internal heating. Significant improvements in conventional heating were shown by the localized hotspots produced by microwave exposure, which accelerated reaction kinetics and increased product yields. The microwave-assisted dyeing process reduced dyeing time by approximately 70% and enhanced dye uptake by 85% compared to conventional infrared heating.

Received 8th December 2025
Accepted 16th January 2026

DOI: 10.1039/d5ra09499b

rsc.li/rsc-advances

Introduction

Azo dyes consist of the chromophore azo group (–N=N–) attached to aromatic auxochromic groups such as hydroxyl (–OH) and primary amino (NH_2) groups.[1] They are among the most common and abundant dyes used in industry due to their simple and cost-effective preparation technique and their wide applications in dyeing textiles, printing, pharmaceuticals, and preparation of metal complexes.[1–4] Among antimicrobial therapeutic agents, sulfa drugs have been known for their antibiotic and antifungal activity. Sulfonamides show other biological activities such as anticancer, anti-inflammatory, anti-convulsant, anti-diuretic, insulin-releasing, anti-hypoglycemic and more.[5] Sulfamethoxazole demonstrated exceptional pharmacological qualities among the sulfonamides, which were of low toxicity, affordability, and noteworthy efficacy against a variety of illnesses.[6,7] Sulfathiazole also showed interesting biological applications.[8] Antibiotics are the most concerning of the drug categories mentioned due to their extensive use and environmental release, which significantly contribute to the global increase in bacterial antibiotic resistance.[5]

Prontosil was the first sulfa-azo dye synthesized drug and used as antibacterial drug which was synthesized by Josel Klarer (1898–1953) and Fritz Mietzsch (1896–1958) in 1932.[9] Several sulfa-azo dyes have been synthesized since the discovery of prontosil aiming to develop more efficient antimicrobial compounds. Synthesis of sulfaguanidine and sulfa-acetamide azo dyes, aryl sulfonamide azo dyes, hetaryl-sulfonamide dyes containing five-membered and six-membered rings have been reported. They showed significant antimicrobial activity.[5]

Designing new drug-like compounds is based on the knowledge of organic, medicinal chemistry, and pharmacology

[a]*Faculty of Women for Arts, Science and Education, Chemistry Department, Ain Shams University, Heliopolis, Cairo, 11757, Egypt. E-mail: Asmaa.Aboelnaga@women.asu.edu.eg*

[b]*Textile Division, National Research Centre, 33 El-Behouth Street, Dokki, P.O. Box 12622, Giza 12522, Egypt*

[c]*Chemistry Department, Faculty of Science, Ain Shams University, Cairo, 11566, Egypt. E-mail: sayed.karam2008@sci.asu.edu.eg*

to form promising drugs in selectivity, potency, and pharmacokinetics aspects.[10] The antimicrobial activity of sulfa drugs occurs by targeting bacterial dihydropteroate synthase (DHPS) and fungal *N*-myristoyltransferase. The sulfonamide targets *para*-aminobenzoic acid (*p*ABA) residues in DHPS which is essential for folate synthesis and bacterial growth.[11,12] The *p*ABA pocket is adjacent to flexible region that can easily mutate and undergo changes which make bacteria resist sulfonamides easily.[13] As bacteria mutates the discovery of new antibacterial is a must.[14] *p*ABA is not only responsible for folate synthesis, also the Pterin play crucial role in the process thus the inhibition can occur at *p*ABA residues or Pterin residues or both. The advantage of Pterin inhibitors over *p*ABA is the rare mutations and bacteria resistance that occur in Pterin interaction site.[15] The *N*-myristoyltransferase (NMT) catalyzes *N*-myristoylation of protein substrates that is essential for directing proteins to membranes and facilitating the formation of protein complexes in fungi and parasites eukaryotic cells.[16,17] The aim is to synthesis dyes that have antimicrobial activity.

Computational studies suggest that increasing steric around sulfonamide (–SO_2–NH–) increases antimicrobial activity. The presence of H-bond donors and acceptors increases the interaction possibility of DHPS thus inhibiting bacterial growth.[18,19] Additionally, charge density distribution may influence antimicrobial activity.[6] Since the sulfa drugs that has been chosen (sulfamethoxazole and sulfathiazole) have free amine group, we have decided to create azo-dyes with antimicrobial activity. The chosen couplers (indan-1-one, indane-1,3-dione, ethylvanillin, and 2,4-dihydroxybenzaldehyde) aimed to investigate the possibility to increase the antimicrobial activity of such dyes. Since indan-1-one, a structural analogue of indane-1,3-dione, has shown significant antimicrobial activity, it is frequently included with indane-1,3-dione in research aimed at the logical creation of new antimicrobial agents.[20] Vanillin, ethyl vanillin, and vanillic acid are examples of phenolic derivatives that have antimicrobial properties by weakening the membranes of bacteria. Vanillin specifically causes cytoplasmic membrane disruption, which allows intracellular contents to leak out of both Gram-positive and Gram-negative bacterial strains, according to research by Fitzgerald *et al.*[21,22] The hydroxyl substituents at positions two and four of 2,4-dihydroxybenzaldehyde in conjugation with azo-triazole moiety were found to be important functional groups that enhance biological activity as well as their ability to coordinate metals (Fig. 1).[23]

Sustainable dyeing is a pressing issue for the apparel and textile industry owing to the swiftly growing environmental distress. It has been observed that the emissions from the garment and textile dyeing industry if left unchecked, can significantly increase by 60% by 2030.[24] Today's growing

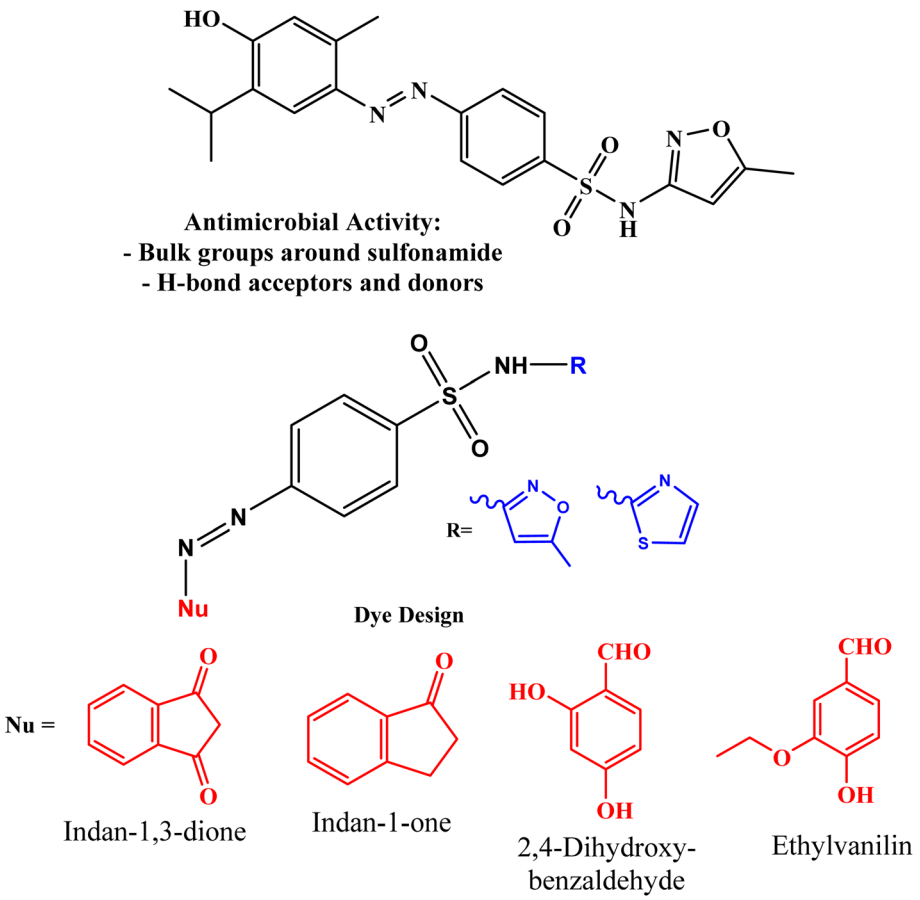

Fig. 1 Dye design approach with antimicrobial activity.

population's demand for textiles is met through the extensive use of textile and apparel dyes that can be toxic, harmful and result in poor dye fixation and many other environmental and ecological issues. The textile industry is dependent on the dyes and the dyeing agents heavily, and this reliance is often hazardous because synthetic dyes often contain harmful chemicals.[25–30] The dyestuff and the finishing processes are a major concern in textile production with the highest use of chemicals, water, and energy among all the previous steps. Moreover, finishing processes are done on textiles after dyeing, increasing the ecological impacts of dyes and dyeing processes. Different techniques are used in the dyeing labs for dyeing fabrics, but traditional methods are both time and energy-consuming.[31–36]

Conventional dyeing methods lose a significant quantity of dyes onto the dye house wastewater because dyes do not exhaust entirely to textiles at room temperature. In addition to these problems, the exhaustion of colors onto synthetic fibers is required to consume high amounts of energy, chemicals, and more time.[37–44] There is worldwide legislative pressure for a reduction in their use: the textile, paper, and leather industries are all included in the Integrated Pollution Prevention and Control Directive. So, there is growing pressure on the dyeing industry to become cleaner worldwide.[45–50] Dyeing energy and practices consumption in the textile industry have increased markedly in prevalence to the demand for sustainable practices. In general, there has been a 415% increase in prices for textiles since 1964 and only a 161% unease in the consumer price index. This has adversely affected the demand for textiles, and the segment expresses the influence of costs throughout the production chain.

This affects the price of textiles and the ecosystem of the textile industry which has started to contract.[51–55] Better quality and choice of life are also demanded by consumers. Textile manufacturers are unsettled both about modification to International Trade laws and the eradication of the Agreement on Textiles and Clothing. All these issues are likely to be aggravated by changes in the industry worldwide resulting from the growth of the industry in developing countries. Each of these principal sponsors also raises several issues relating to the potential, and desirable, role of autoclaves in these changes. Of the various categories of activity in the textile industry, dyeing and finishing processes are considered to have the worst impact on the environment.[56–59]

Reducing environmental pollution, energy consumption, and costs are the main concerns of the textile industry today. In this regard, a more profitable and environmentally friendly dyeing process has been investigated. Many studies indicate that microwave energy can be used efficiently and effectively on textiles in mass processes for the dye and chemical attachment of textile materials. Microwave-assisted dyeing is a developing technology. Microwave energy causes dye exhaustion through increasing temperature and the swelling effect formed in the staple fibers, also enhancing the absorbency in yarn form, both knitted and woven. It was determined that the medium (5 min) and light (3 min) shades for all dyes were obtained quicker with microwave than with the conventional method. Larger amounts of dye could be absorbed in the fabric using microwave energy. The results of microwave energy and conventional processes are similar in terms of color fastness to washing and rubbing. Solar absorptance, thermal effusively, and strength properties are better when treated with microwave energy than with the conventional process.

About 70% of the dye attached to the fabric using the microwave process is as good as 100% of the conventional method. This enhanced efficiency not only reduces the amount of dye required but also minimizes waste and energy consumption, making it a more environmentally friendly option in the textile industry. It has been shown that a model can be created to forecast degrees of dye absorption.[52,60]

Microwave (MW) is a part of the electromagnetic spectrum and covers the frequency range from 300 MHz to 30 GHz. The major advantages of this technology are the short processing time and energy efficiency. The mechanism of microwave energy lies in the interaction of electromagnetic energy with polar or ionic molecules, leading to polar rotations and heat generation. In MW drying and heating, the first heat occurs from the internal part of the material, resulting in quicker heating and a higher evaporation rate of the solvents. The principle of microwave heating is based on heat transfer caused by dipolar molecules positioned in an electromagnetic field created by microwave energy. Process temperature and length can be controlled by microwave application. MW has a positive effect on dye absorption, color yield, fastness properties, and dye bath exhaustion during the dyeing of textile materials. In addition, fiber surface modification also occurs during the MW process, so that the fastness and color yield of dyed fabric with MW are higher than with conventional methods.[61–65]

The current work aims to present a novel way of textile dyeing that uses newly synthesized dyes alongside MW Energy. On one side, newly synthesized dyes are free from toxic and hazardous chemicals and on the other hand, microwave energy provides quick and environmentally friendly dyeing. The research is carried out for a do-it-all purpose, including environment, chemical, sustainable, and other aspects, utilizing modern approaches for textile dyeing and synthesis. Major attention has been given to the development of textile dyes that are chemically synthesized but are environmentally friendly and sustainable. The proposed dyeing method enhances dyeing up to 70% under MW energy instead of 80 min under traditional methods. So, no doubt, shortly, it will substitute the conventional, laborious, and time-consuming techniques by offering eco-friendly, economical, less time-consuming, and enhanced textile dyeing. It is expected that, by implementing this technique, it might become a pragmatic solution for those who have constrained water availability, *i.e.* shortly, not only varied products of textile materials of different patterns and shades will be produced, but with optimal utilization of less water and other resources. The broader outlook of research includes the need for "sustainable and green" strategies to be implemented in the diverse classification of textile industries and the usage of novel, innovative, and conventional methods for the synthesis of materials to be applied during multiple phases of textile dyeing.

The novelty and feasibility of five new synthesized dyes with satisfactory dyeing properties are tested on cotton, wool, silk and polyester (PE) fiber. All fabrics were dyed by applying microwave irradiation using newly synthesized dyes, and the results were compared with those obtained with IR dyeing machine. The MW appliance was used as an alternative irradiation source to afford dyed fabrics in a fraction of the time. The fastness and color measurements were also comparatively evaluated.

Materials and methods

All reagents and solvents used in the study were of commercial grade. Sulfa drugs were sourced from Alpha Chemika. 100% cotton, wool, and polyester were kindly supplied by Misr Company for Spinning and Weaving El-Mehalla El-Kubra, Egypt. 100% silk was obtained from Akhmem, Egypt. $NaBH_4$, sodium triacetate, buffer solution (disodium hydrogen phosphate hydrated), sodium hydroxide, HCl, citric acid, sodium carbonate, ammonia, and ethyl alcohol were of laboratory grade chemicals. Fourier Transform Infrared (FT-IR) Thermo Electron Nicolet iS10 Spectrometer (Thermo Fisher Scientific Inc., Waltham, MA) was used to record spectra (ν, cm^{-1}) using KBr wafer technique. Electron impact mass spectra (EI-MS) were run on direct probe controller inlet part to single quadrupole mass analyzer in (Thermo Scientific GC-MS) MODEL (ISQ LT) employing Thermo X-CALIBUR software at regional center for mycology and biotechnology (RCMB), Al-Azhar University, Cairo, Egypt. ^1H and ^{13}C NMR spectra (δ, ppm) were performed on BRUKER (400 and 100 MHz) spectrometer at Faculty of Science, Zagazig University, Egypt, respectively, with tetramethyl silane (TMS) as an internal standard, using DMSO-d_6 as a solvent. The elemental analyses were run using a PerkinElmer 2400 CHN elemental analyzer (PerkinElmer, Waltham, MA) at Faculty of Science, Ain Shams University.

Azodye synthesis

A suspension of sulfathiazole (0.1 mmol) in HCl (10 mL, 6 N) was prepared, and an ice-cold solution of sodium nitrite ($NaNO_2$, 3 mmol, 2.56 g, 100 mL) was added dropwise over 30 min while maintaining the temperature at 0–5 °C. This reaction generated the corresponding diazonium salt, which was then slowly introduced into a cold solution containing the selected coupler (1,3-indandione, 1-indanone, 2,4-dihydoxybenzaldehyde, ethylvanillin) dissolved in NaOH. The reaction mixture was maintained under stirring in an acidic medium at the same temperature for 1 h. The resulting solid was collected by filtration, thoroughly washed with distilled water, air-dried, and subsequently purified by recrystallization using ethanol and 1,4-dioxane (2 : 1) to obtain the pure compounds.

4-[2-(5-Formyl-2,4-dihydroxyphenyl)diazen-1-yl]-*N*-(5-methyl-1,2-oxazol-3-yl)benzene-1-sulfonamide (3a). Dark-red solid, MP. 190–191 °C; yield: 88%; IR (KBr) ν, cm^{-1}: 3159 (br. O–H, NH), 1640 (C=O), 1469 (N=N), 1311 (SO_2), 1160 (C–O); ^1H NMR (400 MHz, DMSO-d_6): δ (ppm): 2.30 (s, 3H, CH_3 of methoxazole ring), 6.31 (s, 1H, methoxazole), 7.20 (s, 1H, C3–H, dihydroxyphenyl), 7.55–7.75 (m, 5H, Ar–H), 8.14 (br.s, 2H, OH, exchangeable), 9.92 (s, 1H, CHO), 11.50 & 11.75 (br.s, 1H, NH, hydrazo and azo tautomers 1 : 3, exchangeable); ^{13}C NMR (100 MHz, DMSO-d_6) δ (ppm): 12.0, 95.4, 102.1, 108.6, 126.0, 126.6 (2), 127.6 (2), 127.9, 128.8, 129.4, 131.7, 132.7, 157.4, 160.4, 170.4; EI-MS, (m/z, %): 402.67 ($M^{+\bullet}$, 19.9%), 328.33 (100%); anal. calc. for $C_{17}H_{14}N_4O_6S$ (402.38): C, 50.74; H, 3.51; N, 13.92; found: C, 50.62; H, 3.43; N, 13.91%.

4-[2-(1,3-Dioxo-2,3-dihydro-1*H*-inden-2-yl)diazen-1-yl]-*N*-(5-methyl-1,2-oxazol-3-yl)benzene-1-sulfonamide (4a). Yellow solid, MP. 276–278 °C; yield: 95%; IR (KBr) ν, cm^{-1}: 3192 (NH), 1712 (C=O), 1475 (N=N), 1356 (SO_2), 1158 (C–O). ^1H NMR (500 MHz, DMSO-d_6): δ (ppm): 2.28 (s, 3H, CH_3 of methoxazole ring), 3.82 (s, 1H, indandione-H), 6.12 (s, 1H, methoxazole), 7.42–7.79 (m, 8H, Ar–H), 10.78 & 11.27 (br.s, 1H, NH, hydrazo and azo tautomers 1 : 3, exchangeable); ^{13}C NMR (100 MHz, DMSO-d_6) δ (ppm): 12.1, 29.6, 95.4, 113.8, 123.3, 127.1, 127.9, 128.8 (2), 130.8 (2), 135.2, 138.0, 143.6, 146.2, 148.1, 157.7, 170.3, 189.1; EI-MS, (m/z, %): 410.40 ($M^{+\bullet}$, 22.2%), 297.35 (100%); anal. calc. for $C_{19}H_{14}N_4O_5S$ (410.40): C, 55.61; H, 3.44; N, 13.65; found: C, 55.53; H, 3.39; N, 13.63%.

4-((1,3-Dioxo-2,3-dihydro-1*H*-inden-2-yl)diazenyl)-*N*-(thiazol-2-yl)benzenesulfonamide (4b). Green solid, MP. 278–280 °C, yield: 90%; IR (KBr) ν, cm^{-1}: 3282 (N–H stretching), 1718 (C=O), 1408 (N=N), 1325 (SO_2 vibrational asymmetric and symmetric), 1141 (C–O); ^1H NMR (500 MHz, DMSO-d_6): δ (ppm): 3.38 (s, 1H, indandione), 6.83 (d, 1H, thiazole, J = 5.0 Hz), 7.26 (d, 1H, thiazole, J = 5.0 Hz), 7.73 (d, 2H, Ar–H, J = 9.0 Hz), 7.84 (d, 2H, Ar–H, J = 8.5 Hz), 7.89–7.92 (m, 4H, Ar–H), 12.75 & 13.08 (br.s, 1H, NH, hydrazo and azo tautomers 1 : 3, exchangeable); ^{13}C NMR (100 MHz, DMSO-d_6) δ (ppm): 39.5 (CH indandione), 116.1, 116.2, 122.8, 122.9, 124.3, 124.6, 127.5, 127.7, 132.3, 135.7, 135.8, 138.2, 138.9, 140.3, 144.6, 168.7, 185.5, 186.4; EI-MS, (m/z, %): 412.19 ($M^{+\bullet}$, 20.6%), 64.26 (100%); anal. calc. for $C_{18}H_{12}N_4O_4S_2$ (412.44): C, 52.42; H, 2.93; N, 13.58; found: C, 52.31; H, 2.82; N, 13.59%.

***N*-(5-Methyl-1,2-oxazol-3-yl)-4-[(1*E*)-2-(1-oxo-2,3-dihydro--1*H*-inden-2-yl)diazen-1-yl]benzene-1-sulfonamide (5a).** Yellow solid, MP. 250–252 °C, yield: 87%; IR (KBr) ν, cm^{-1}: 3175 (N–H), 1680 (C=O), 1475 (N=N), 1334 (SO_2), 1162 (C–O); ^1H NMR (500 MHz, DMSO-d_6): δ (ppm): 2.07 (d, 2H, CH_2 of indanone, J = 6.0 Hz), 2.28 (s, 3H, CH_3 of methoxazole ring), 3.82 (t, 1H, indanone-H, J = 6.0 Hz), 6.12 (s, 1H, methoxazole-H), 7.43–7.79 (m, 8H, Ar–H), 10.79 & 11.27 (br.s, 1H, NH, hydrazo and azo tautomers 1 : 3, exchangeable); ^{13}C NMR (100 MHz, DMSO-d_6) δ (ppm): 12.1, 29.6, 95.4, 99.6, 113.9, 123.4, 127.2, 128.9 (2), 130.9 (2), 135.3, 138.0, 143.6, 146.2, 148.1, 157.7, 170.4, 189.2; EI-MS, (m/z, %): 396.29 ($M^{+\bullet}$, 28.4%), 173.07 (100%); anal. calc. for $C_{19}H_{16}N_4O_4S$ (396.42): C, 57.57; H, 4.07; N, 14.13; found: C, 57.68; H, 4.01; N, 14.15%.

4-[2-(1-Oxo-2,3-dihydro-1*H*-inden-2-yl)diazen-1-yl]-*N*-(1,3-thiazol-2-yl)benzene-1-sulfonamide (5b). Red solid, MP. 192–194 °C, yield: 80%; IR (KBr) ν, cm^{-1}: 3139 (N–H), 1700 (C=O), 1475 (N=N), 1329 (SO_2), 1141 (C–O); ^1H NMR (500 MHz, DMSO-d_6): δ (ppm): for azo tautomer (66%): 2.62 (d, 2H, CH_2 of indanone, J = 6.0 Hz), 3.08 (t, 1H, H of indanone, J = 6.0 Hz),

6.82 (d, 1H, J = 5.0 Hz, thiazole), 7.25 (d, 1H, J = 5.0 Hz, thiazole), 7.39–7.80 (m, 8H, Ar–H's), 12.75 (br.s, 1H, NH); for hydrazo tautomer (33%): 3.40 (s, 2H, CH_2 of indanone), 13.05 (br.s, 1H, NH); ^{13}C NMR (100 MHz, DMSO-d_6) δ (ppm): 25.4 (azo), 29.5 (hydrazo), 35.9, 112.6, 113.6, 122.9, 123.2, 124.5, 127.1, 127.3, 127.5, 127.8, 134.7, 135.1, 136.7, 142.8, 146.1, 147.1, 152.1, 168.8; EI-MS, (m/z, %): 398.67 ($M^{+\bullet}$, 51.9%), 69.04 (100%); anal. calc. for $C_{18}H_{14}N_4O_3S_2$ (398.46): C, 54.26; H, 3.54; N, 14.06; found: C, 54.11; H, 3.52; N, 14.05%.

4-[(1*E*)-2-(3-Ethoxy-5-formyl-2-hydroxyphenyl)diazen-1-yl]-*N*-(5-methyl-1,2-oxazol-3-yl)benzene-1-sulfonamide (6a). Pale-yellow solid, MP. 184–186 °C, yield: 88%; IR (KBr) ν, cm^{-1}: 3362 (br. OH), 3153 (N–H), 1686 (C=O), 1442 (N=N), 1378 (SO_2), 1164 (C–O–C); ^{1}H NMR (500 MHz, DMSO-d_6): δ (ppm): 1.33 (t, 3H, CH_3 of ethyl, J = 6.5 Hz), 2.49 (s, 3H, CH_3 of methoxazole ring), 4.05 (q, 2H, J = 7 Hz, CH_2 of ethyl), 6.08 (s, 1H, methoxazole), 6.978–7.997 (m, 6H, Ar–H's), 8.00 (br.s, 1H, OH), 9.73 (s, 1H, CHO), 11.08 (br.s, 1H, NH). ^{13}C NMR (100 MHz, DMSO-d_6) δ (ppm): 12.1, 14.7, 63.9, 95.4, 111.8, 114.8, 115.5 (2), 126.0, 126.7, 128.8, 128.9 (2), 147.4, 150.4, 153.3, 157.9, 170.1, 191.2; EI-MS (m/z, 100%): 430.00 ($M^{+\bullet}$, 19.6%), 371.5 (100%); anal. calc. for $C_{19}H_{18}N_4O_6S$ (430.44): C, 53.02; H, 4.22; N, 13.02; found: C, 53.13; H, 4.17; N, 13.07%.

Dyeing process

Before using, the fabrics were scoured in aqueous solution containing (3 g L^{-1}) non-ionic detergent (Hostapal, Clariant, Swiss) and 2 g L^{-1} of sodium carbonate at 60 °C for 30 min then the fabric was thoroughly rinsed with cold water and finally dried at ambient temperature.

Microwave-assisted dyeing process

The cotton, wool, silk, as well as polyester fabrics, were dyed under microwave irradiation at different pH (3, 7, 9), contain various concentrations (0.5, 1, 1.5, and 2 g/100 mL H_2O), different watts (60, 70, 80, 90) for different times (5, 10, 15, 20, and 30 min). Before dyeing process, the weighted dye dissolved in 1 mL ethyl alcohol the added hot distilled water with well shaking to ensure good and uniform distribution of the dye. Upon completing the dyeing process, the dyed fabrics underwent thorough washing under running water. Subsequently, they were soaked in a new bath containing a concentration of 1 g L^{-1} of soap, classified as a nonionic detergent, for a duration of 15 min at a temperature of 60 °C. This was followed by multiple rinses with water, after which the fabrics were dried at room temperature.

Analysis and characterization of dyed fabrics

Colorimetric measurements. The dyed fibers' reflectance values (K/S) were established by employing the un-dyed white fibers as a reference blank. This assessment was conducted using a Hunterlab Colorimeter, specifically the Model SpectroEye X-rite, in conjunction with applied of the Kubelka–Munk equation.[66]

$$\frac{K}{S} = \frac{(1-R)^2}{2R} \quad (1)$$

where, K/S = color strength values of the samples, K = absorption coefficient, S = light scattering coefficient, and R = surface reflectance value at a particular wavelength where maximum adsorption occurs.

Color fastness

Rubbing fastness. The assessment of color fastness to rubbing was conducted following the AATCC test method [AATCC 8, 1993]. This procedure involved the transfer of color from the surface of the dyed fabric to an alternate surface through the act of rubbing. A colored test specimen, securely attached to the base of a crock meter, was subjected to friction against a white crock test cloth under regulated conditions.[67,68]

Dry rubbing test. The test specimen was positioned on the base of the crock meter, with a white testing cloth affixed above it. A covered finger was subsequently lowered onto the test specimen, initiating a sliding motion back and forth. This process involved ten complete rotations, performed at a rate of one rotation per second, totaling 20 movements. Following this procedure, the white test sample was extracted for assessment utilizing the Grey Scale to determine the extent of staining.[69]

Wet rubbing test. The white test sample was completely immersed in water, achieving a 65% uptake. This process was executed by previous protocols, and subsequently, the white test samples were allowed to air dry before assessment.[54]

Washing fastness. The evaluation of color fastness to washing was conducted following the AATCC test method [AATCC 36, 1993], utilizing a Launder-Ometer. Specimens dimensions 5 × 10 cm were affixed between two identical strips of bleached cotton fabric. This composite specimen was subsequently submerged in an aqueous solution comprising 5 g L^{-1} of soap and 2 g L^{-1} of sodium carbonate, maintaining a liquor ratio 50 : 1. The bathing solution was maintained at a controlled temperature of 95 °C.

The experiment was conducted for 30 minutes at a rotational speed of 42 rpm. Subsequently, the samples were extracted, subjected to two rinsing procedures that involved periodic stirring or manual wringing, and dried. The evaluation of washing fastness was carried out by referencing the Grey Scale to measure any color changes.[70]

Perspiration fastness

Alkaline perspiration. A solution was prepared by dissolving 0.25 g L^{-1} of L-histidine monohydrochloride monohydrate along with 10 g L^{-1} of sodium chloride and 1 g L^{-1} of sodium dihydrogen phosphate in one liter of distilled water. Subsequently, the pH of the solution was modified to 4.3 using a 10% acetic acid solution. The specimen, measuring 5 × 4 cm and exhibiting color, was positioned between two uncolored specimens to create a composite sample. This composite was subsequently submerged in each solution for a duration of 15 to 30 min, during which intermittent agitation and squeezing were employed to guarantee thorough wetting of the materials.

The test specimen was positioned between two glass plates and subjected to a force of approximately 4–5 kg. Subsequently, these plates, which housed the composite specimen, were oriented vertically and maintained in an oven at a temperature of 37 °C ± 2 for 4 h, by the AATCC 15 standard established in 1993. The resultant impact on the coloration of the test specimen was evaluated and quantified by utilizing the Grey Scale method for assessing color change.[71]

Light fastness. The assessment of color fastness to light was conducted following the AATCC test method 16 A-1989. This evaluation utilized the blue scale as a benchmark for measuring color change, as specified in AATCC 16A (1993).[70]

Assessment of antimicrobial activity

Molecular docking. The molecular docking was performed using drug design program.[72] The novel six dyes were docked against bacterial dihydropteroate synthase of *Yersinia pestis* (PDB: 3TZF) and *N*-myristoyltransferase of *Candida albicans* fungus (PDB: 1IYL).[73] The results were compared to co-crystallized ligands of both proteins. The six dyes were built using SMILES format in the program and have been energy minimized and adjusted for partial charges. The proteins were prepared by water removal for NMT protein, on the other hand, the water molecules in DHPS were retained since it has role in the interaction.[13] The hydrogen atoms were added for both; correction and energy minimization were applied for both. The desired pockets were later isolated with co-crystalized ligand in each protein. All the six dyes and the co-crystallized ligands were imported into database and the docking performed at ligand atoms.

Assessment of antimicrobial activity on fabric

Antimicrobial activity assessment was conducted using two bacterial strains: *E. coli* ATCC 11229 (Gram-negative) and *S. aureus* ATCC 6538 (Gram-positive). Additionally, two fungal strains, *A. niger* and *C. albicans*, were included in the study. The selected bacterial strains are commonly associated with wound infections. Fresh inoculates for antibacterial evaluation were cultivated in nutrient broth at 37 °C for 24 h.

In this investigation, the agar colony counting method was employed. The antibacterial efficacy of the compounds was evaluated against *S. aureus*, a Gram-positive bacterium, and *E. coli*, a Gram-negative bacterium. A liquid culture was created by dissolving 0.5 g of peptone and 0.3 g of beef extract in 100 mL of water. Fabric samples, each with a diameter of 1 cm, were cut and immersed in 10 mL of the liquid culture, to which 10 μl of microbial culture was added. All samples were incubated for 24 h at 37 °C. Following the incubation period, 100 μl from each sample solution was diluted and plated onto agar plates. These plates were then further incubated for another 24 h, after which the resulting colonies were counted. The percentage reduction of bacteria was calculated using a specified formula.

$$\text{Reduction in CFU\%} = \frac{C - A}{C} \times 100 \quad (2)$$

where A is CFU mL^{-1} after contact (end test) and C is CFU mL^{-1} at zero contact time.[74,75]

Results and discussion

Chemistry

In the current study, sulfamethoxazole and sulfathiazole underwent diazotization reaction to form sulfa-azo dyes. The reaction occurred in acidic conditions where diazonium salt of sulfa drug is formed then coupled with electron-donating (nucleophile) couplers which are; indan-1-one, indane-1,3-dione, ethylvanillin, and 2,4-dihydroxybenzaldehyde (Scheme 1). The resulting azo dyes confirmed their molecular structures by IR, ^{1}H NMR, ^{13}C NMR, UV, and mass spectroscopy analysis.

IR spectra provided key functional group information. The presence of characteristic absorption bands confirms the successful formation of the target molecules. The N–H stretch in the sulfonamide group is consistently observed in the range of 3090–3185 cm^{-1}, confirming the presence of this moiety in all compounds. A strong band around 1440–1475 cm^{-1} is attributed to the N=N azo linkage. This is a crucial piece of evidence for the successful diazo coupling reaction. The S=O asymmetric and symmetric stretches of the sulfonamide group (SO_2) appear as strong bands typically in the 1311–1356 cm^{-1} and 1141–1162 cm^{-1} regions, respectively. The presence of C=O stretches is evident in compounds containing ketone or aldehyde groups.

Compounds **4a**, **4b**, **5a**, **5b**, and **6a** show strong C=O bands at ν 1712, 1718, 1680, 1700, and 1686 cm^{-1}, respectively. Compound **3a** showed a C=O stretch at 1640 cm^{-1}, characteristic of an aldehyde conjugated with a benzene ring. The O–H stretch at 3159 cm^{-1} in compound **3a** and 3362 cm^{-1} in **6a** confirms the presence of hydroxyl groups. NMR data is vital for confirming the molecular skeleton and the arrangement of atoms. Aromatic protons (Ar–H): all compounds show a complex multiplet or a series of doublets in the aromatic region (6.0–8.0 ppm), corresponding to the benzene rings of the sulfonamide and the coupled moieties. The number of aromatic protons matches the expected structure. Sulfonamide N–H: a broad singlet is observed in the downfield region (10.7–12.7 ppm), confirming the presence of the exchangeable sulfonamide proton. The methyl groups on the methoxazole ring (**3a**, **4a**, **5a**, **6a**) and the ethyl group in **6a** are clearly visible. For **4a** and **5a**, a doublet at 2.28 ppm with a characteristic coupling constant confirms the methyl group on the methoxazole ring. In **6a**, a triplet at 1.33 ppm and a quartet at 4.05 ppm confirm the ethyl group.

Azo dyes, particularly those with a hydroxyl or amine group *ortho* or *para* to the azo linkage, can exist in a tautomeric equilibrium between the azo and hydrazo forms. The infrared (IR) spectra provide the primary evidence for this tautomeric equilibrium as in compound **4a**, the presence of a broad band around 3200 cm^{-1} and a weaker band around 1660 cm^{-1} can be attributed to the stretching vibrations of the N–H and C=N bonds, respectively. These signals are characteristic of the hydrazone tautomer. While the presence of a strong band around 1460 cm^{-1}, assigned to the N=N stretching vibration, confirms the existence of the azo

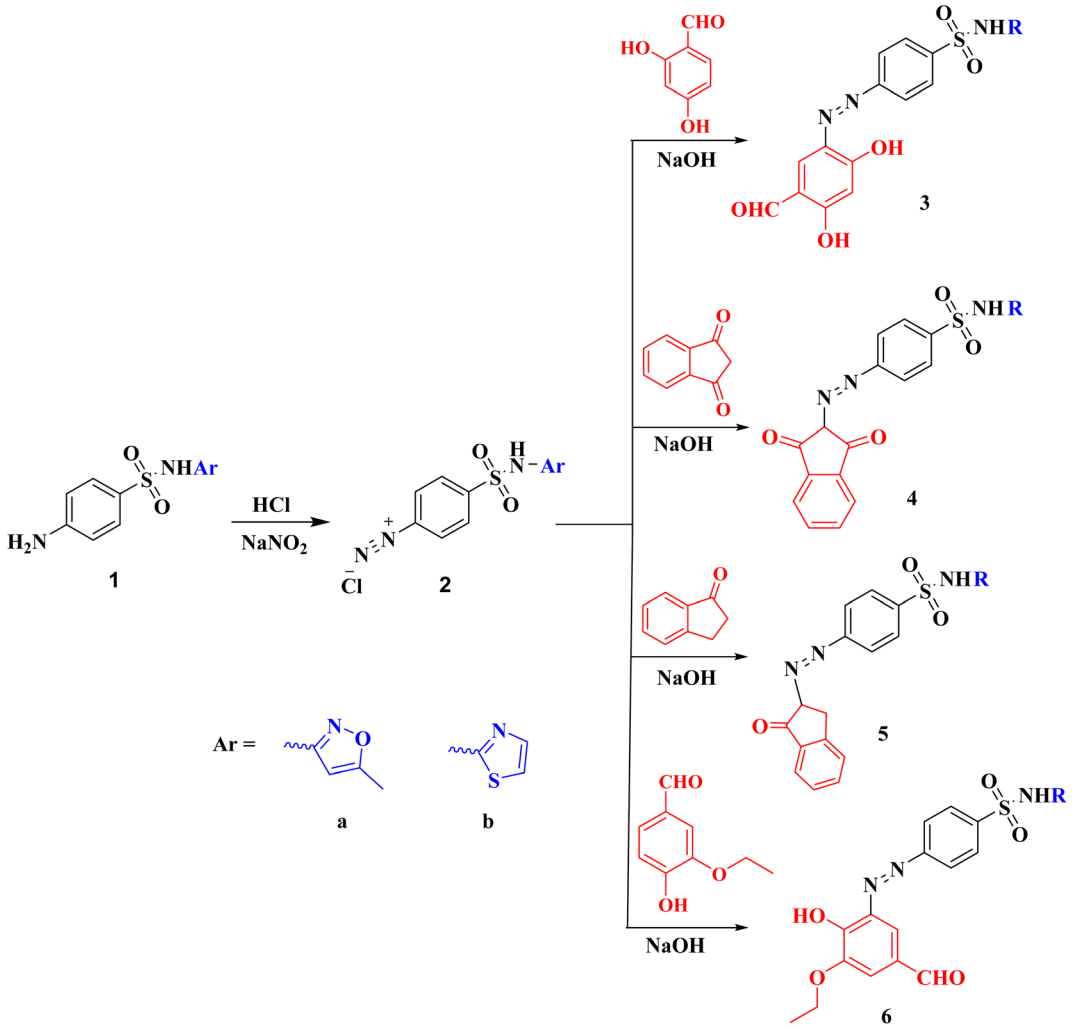

Scheme 1 Schematic synthesis for sulfa-azo dyes.

tautomer. Further support comes from ^{1}H NMR spectrum for compounds **4a** and **4b** suggests the existence of two different NH protons, each with a different electronic environment. In compound **4a**, the signal at δ 12.75 ppm is likely from the sulfonamide N–H proton, and at δ 13.08 is likely from the sulfonamide N–H proton, his proton is involved in a very strong intramolecular hydrogen bond, which causes significant deshielding and shifts its signal far downfield.[64]

The ^{13}C NMR spectra showed the correct number of signals corresponding to the unique carbon environments in each molecule. The C=O carbons of the indandione and indanone rings are clearly identified in the downfield region (185–189 ppm). The two C=O carbons in the symmetrical indandione ring (**4a** and **4b**) appear as distinct signals. In thiazole-based dyes (**4b** and **5b**), the C=N signal appears at approximately 168 ppm, whereas in methoxazole-based dyes it appears at approximately 157 ppm. The higher chemical shift in the thiazole derivatives is attributed to the electron-withdrawing effect of the sulfur atom, which increases the deshielding of the adjacent C=N carbon. In contrast, the oxygen in methoxazole is less electron-withdrawing than sulfur, resulting in a slightly lower chemical shift for the C=N carbon. The C=C carbons of both the heterocyclic and aromatic rings were observed in the range of 110–140 ppm. Mass spectrometric analysis, which indicated the presence of the corresponding molecular ion peaks ($M^{+\bullet}$), finally provided conclusive confirmation of the structural elucidation of the synthesized azo dyes, validating the successful formation of the target dye compounds.

UV-vis spectral analysis

The UV-vis absorption spectra of compounds **3a**, **4a**, **4b**, **5a**, **5b**, and **6a** were recorded in the range of 320–460 nm, as shown in Fig. 2. All compounds exhibited characteristic absorption bands assigned to $\pi \rightarrow \pi^*$ transitions of the azo–aromatic chromophore, with slight variations in λ_{max} and intensity reflecting differences in their electronic environments. Compound **3a** displayed the most intense absorption with λ_{max} at 374 nm, while **4a** showed a slightly blue-shifted band at 360 nm. A significant bathochromic shift was observed for **4b** (λ_{max} = 420 nm), indicating enhanced conjugation and a stronger electron-donating effect of its substituent. In contrast, **5a** exhibited the weakest absorption with λ_{max} at 350 nm. This reduction suggests either

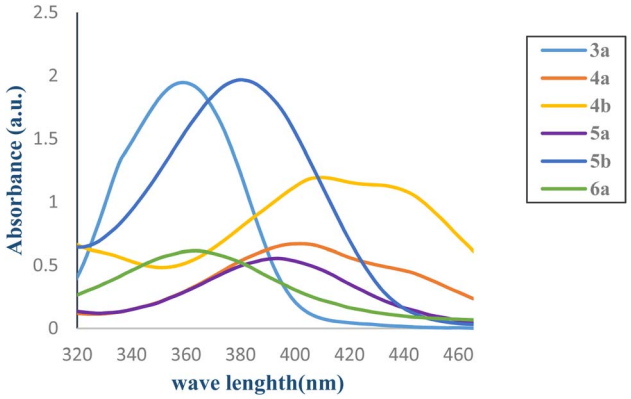

Fig. 2 UV-vis absorption spectra of dyes **3–6**(a–b).

transitions with have a larger n → π* character or with a less-conjugated geometry making the π → π* transition weaker. n → π* transitions are typically lower in intensity because they are symmetry-forbidden or less allowed than π → π*. Whereas its analogue **5b** showed a moderate red shift and higher intensity at 382 nm. Compound **6a** presented a broad band centered at 355 nm with a shoulder extending toward higher wavelengths, suggesting possible intramolecular hydrogen bonding or overlapping π → π* and n → π* transitions.[76]

Overall, the "**b**" derivatives displayed red-shifted and more intense absorptions compared to their "**a**" analogue, confirming that substitution on the heterocyclic moiety significantly influences the electronic transition energies. These observations indicate that the optical properties of the synthesized azo compounds are primarily governed by the degree of π-conjugation and the electron-donating or withdrawing nature of the substituents attached to the azo linkage.[77]

Moreover, the DFT-calculated frontier molecular orbital (FMO) energies correlate well with the experimental UV-vis spectra, as *vide infra*. Among the studied dyes, compound **4b** has the smallest HOMO–LUMO gap (ΔE = 3.154 eV), suggesting enhanced intramolecular charge transfer. This theoretical prediction aligns with the experimental results, where **4b** exhibits the longest absorption wavelength (λ_{max} = 420 nm), confirming the accuracy of the DFT model in describing the electronic transitions.

Dyeing

Textile dyeing is known as one of the most polluting industries in the world due to the high-water consumption as well as the high amount of chemicals and energy used. Therefore, the current study has focused on the evaluation of newly synthesized dyes derived from natural compounds and their performance combined with microwave energy, which reduces water and chemicals consumption, energy use, and process time, and the new dyes are eco-friendly.

Effect of the dyeing bath pH on dye absorption

Fig. 3 illustrates the cumulative impact of dyeing path pH factors (**3**, **7**, and **9**), on the concurrent dyeing mechanism of cotton, wool, silk and polyester fabrics with applying microwave irradiation as a heating source (1% shade at 90 watt for 5 min).

From the finding in Fig. 1 say that the three variables have a significant impact on the effectiveness of dyeing (dye bath pH, synthesized dye, and fabric structure), the color hue depended on dye bath pH and fabric type as well as dye structure, the highest color strength (*K*/*S*) was obtained at dye path pH 7 (neutral pH), protein fabrics (wool and silk fabric) has the highest *K*/*S* value while cotton fabric has the lowest one and follow the following order: wool > silk > polyester > cotton.

Dyeing technique and dye-fabric bond formation

The process of dyeing involves a series of interactions between dye molecules and textile fibers, resulting in the formation of bonds that are essential for color retention and stability. Understanding these dye-fiber bonds is critical to analyzing the effectiveness of different dyeing techniques and the types of fibers used. Various factors such as temperature, pH, and the chemical structure of both the dye and the fiber play significant roles in determining the strength and durability of these bonds. Employing specific conditions can optimize the dyeing process, leading to improved colorfastness and overall quality of the dyed fabric. Consequently, a thorough examination of the dyeing process and the dynamics of dye-fiber interactions is fundamental for advancements in textile dyeing technology.

In exhaust dyeing, a limited number of fabrics being analyzed are submerged in a solution containing newly synthesized dyes. Throughout the dyeing procedure, the fabric remains in the dye bath for a predetermined duration, which allows the dye molecules to transfer from the solution to the textile substrate over time. This stage, referred to as exhaustion, is succeeded by the absorption and fixation of the dye within the fiber structure. The effectiveness of these stages is systematically regulated by managing dyeing conditions, particularly the temperature, which is generally kept at 80 °C for cellulose fabric (cotton) and protein fabrics (wool and silk fabric), while it is maintained at 130 °C for polyester fabric for 30 min when using IR technique. While at 90% watts, 1% shade and pH 7 for 5 min, when applying microwave irradiation as a heating source.

The synthesized dye (**3a** and **4a**) exhibits a chemical structure with a backbone that integrates the chromophoric group (–N=N–) and the autochromic group (–OH). The resultant color of this dye arises from the interaction between the (–N=N–) bond and the corresponding chromophore (–OH). Both dyes can react with cotton, wool, and silk fabrics by substitution reaction and forming hydrogen bond between dye and fabrics.[78]

The process of dyeing fabrics using the other synthesized dyes (**4b**, **5a**, **5b**, and **6a**) can be divided into three critical stages: adsorption, penetration, and fixation. In the first stage, known as adsorption, dye molecules transition from the dye bath to the surface of the fiber, establishing a superficial layer *via* physical adsorption. This initial layer is crucial for the dyeing process, as it sets the stage for further dye uptake; additional adsorption is contingent upon the dye molecules' ability to penetrate further into the fiber structure.[78,79]

In the second phase, known as diffusion or penetration, the dye molecules that have adhered to the surface begin to infiltrate the internal structure of the fiber, systematically

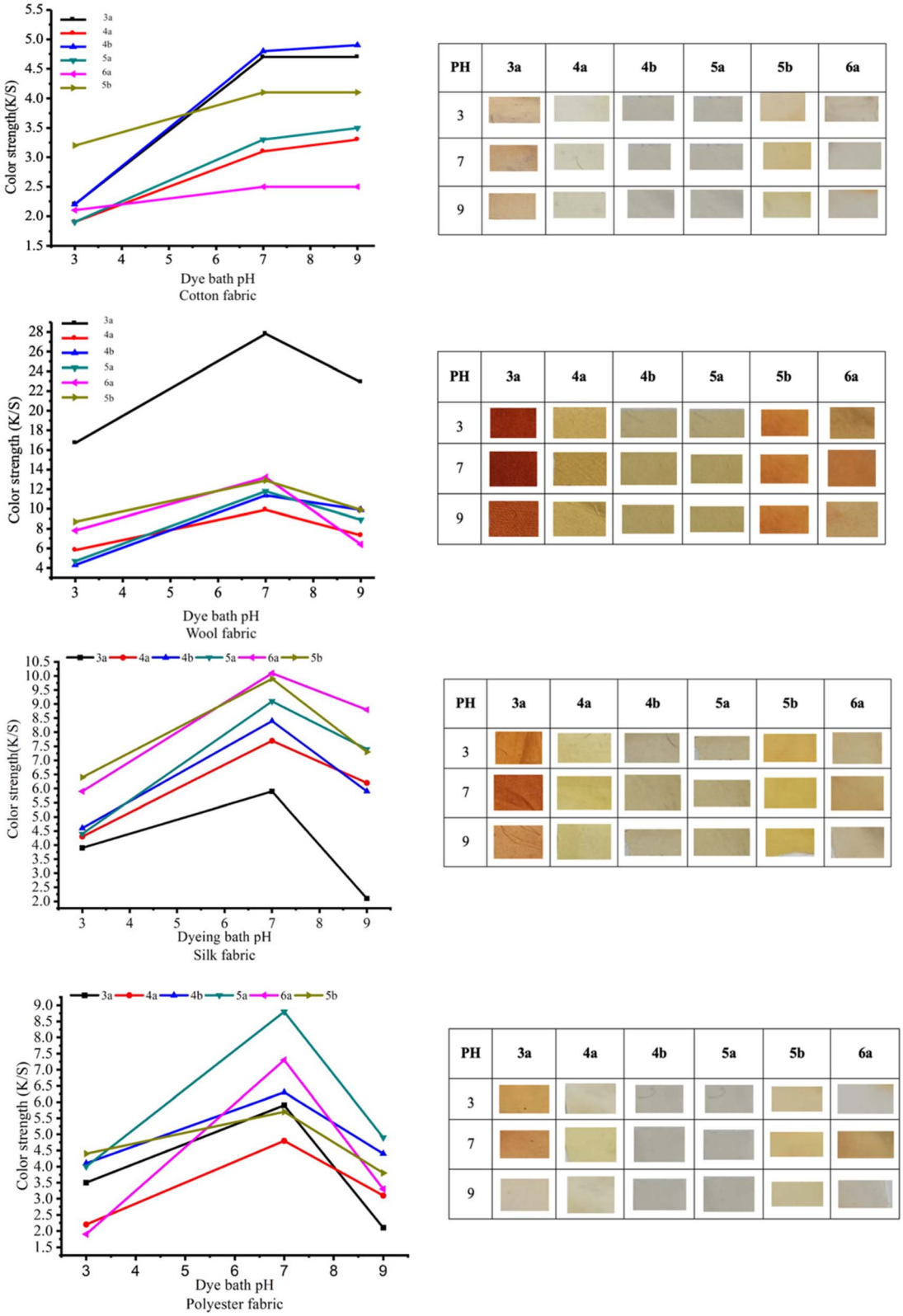

Fig. 3 The combined effect of dyeing bath pH of cotton, wool, silk and polyester fabric dyed with newly synthesized dyes assisted by MW irradiation.

permeating its pores and channels. The extent and effectiveness of this penetration are contingent upon several factors, such as the molecular properties of the dye, the structural organization of the molecules within the fiber, and the specific parameters of the dyeing process. The success of this diffusion process is vital for producing rich and long-lasting colors; inadequate

penetration may result in muted hues and diminished color fastness.

In the final phase (dye fixation), the dye molecules identify and adhere to distinct binding sites within the fiber. The forces responsible for maintaining the attachment of these dye molecules can be diverse, encompassing van der Waals forces and hydrogen bonds. The molecular configuration of the newly synthesized dyes presents numerous interaction opportunities with the fabric substrate. Notably, the azo groups are capable of engaging in dipole–dipole interactions with the functional groups present in the polymer. Furthermore, the hydroxyl group offers potential for hydrogen bonding with the carbonyl oxygen atoms found in the fabric. Moreover, the presence of an extensive conjugated system within these dyes promotes van der Waals (VDW) interactions and may enable π–π stacking with the aromatic components of the polymer.

Effect of the dyeing bath temperature (watt) on dye absorption

The influence of dye path temperature on dyeing of fabrics under study was systematically examined across various watts (70, 80, and 90). The data presented in Fig. 4 and 5 indicated a clear trend: as the Watt rose from 70 to 90 watts, the color strength, measured by the *K*/*S* ratio, increased. At lower watts, the dyed fabrics exhibited a bright hue. However, with an increase in watts, the aggregation of dye molecules diminished, facilitating a more effective and rapid diffusion of the synthesized dye into all fabrics. This process leads to notable lightness, saturation, and overall color differentiation variations. The findings suggest that the microwave heating method yields the highest *K*/*S* value at 80 watts for wool and silk fabric, followed by cotton and polyester fabric at 90 watts. Therefore, it is evident from the data that an increase in temperature (watts) positively correlates with the enhancement of color strength in fabrics.

Effect of the dyeing time on dye absorption

Fig. 6 presents the *K*/*S* values for dyed cotton, wool, silk, and polyester fabrics using MW irradiation obtained from synthesized dyeing namely (**3a**, **4a**, **4b**, **5a**, **5b**, and **6a**), at varying dyeing duration. The findings indicate that the microwave heating method achieved a higher *K*/*S* value 20 min for wool and

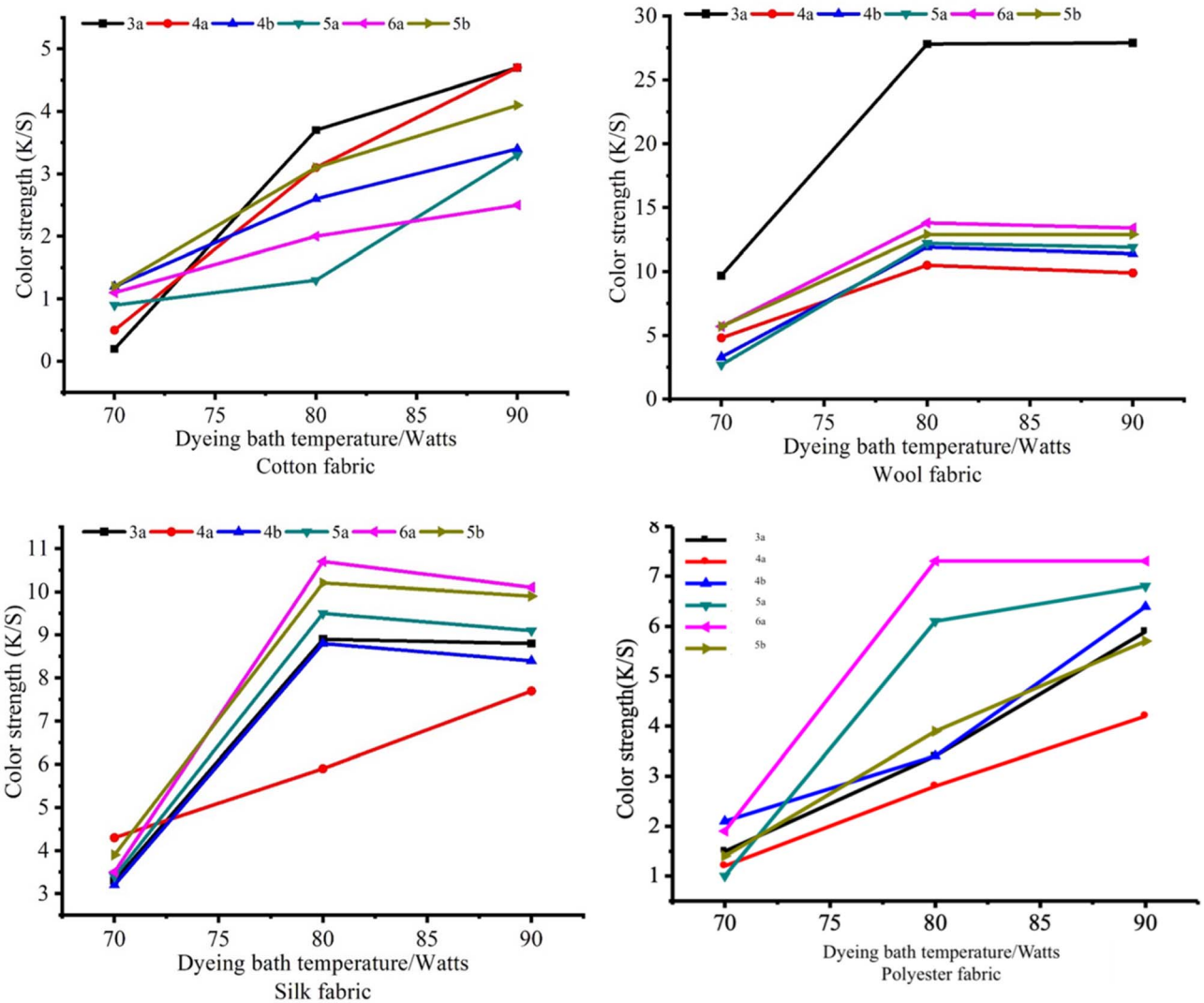

Fig. 4 The combined effect of dyeing bath temperature (watts) of cotton, wool, silk, and polyester fabric assisted by MW irradiation.

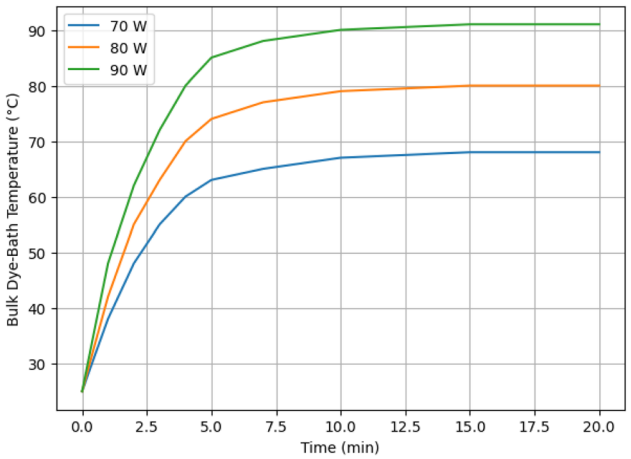

Fig. 5 Temperature/time of dye bath under different MW power.

silk fabric and 30 min for cotton and polyester fabrics. The figure further suggests that *K*/*S* values generally increased with extended dyeing time. This increase may be linked to the effects of MW irradiation, which assists in the penetration of color into the fabric and enhances the depth of infiltration.

Impact of the dye concentration on dye absorption

Fig. 7 presents the results of *K*/*S* ratios for dyed fabrics under study with synthesized dyes, utilizing MW irradiation, at varying dye concentrations (1, 1.5, 2%) according to the fabrics weight. The findings indicate that MW irradiation achieved the highest *K*/*S* ratio of wool and silk at a dye extract concentration of 1.5 g/100 mL. This was followed by cotton and polyester fabric, at a concentration of 2 g/100 mL. It is noted that high concentration demonstrated higher *K*/*S* values but was observed to result in a harsher fabric filling.

From all the above results we can say that the optimum condition for dyeing wool and silk fabric is (1.5% shad, for 20 min at 80 watt), while for cotton and polyester fabric is (2% shad, for 30 min at 90 watt) at pH 7 for all fabrics. For a comparison we dyed the same fabric and dyes by applying infrared (IR) as a heating source at the optimum condition

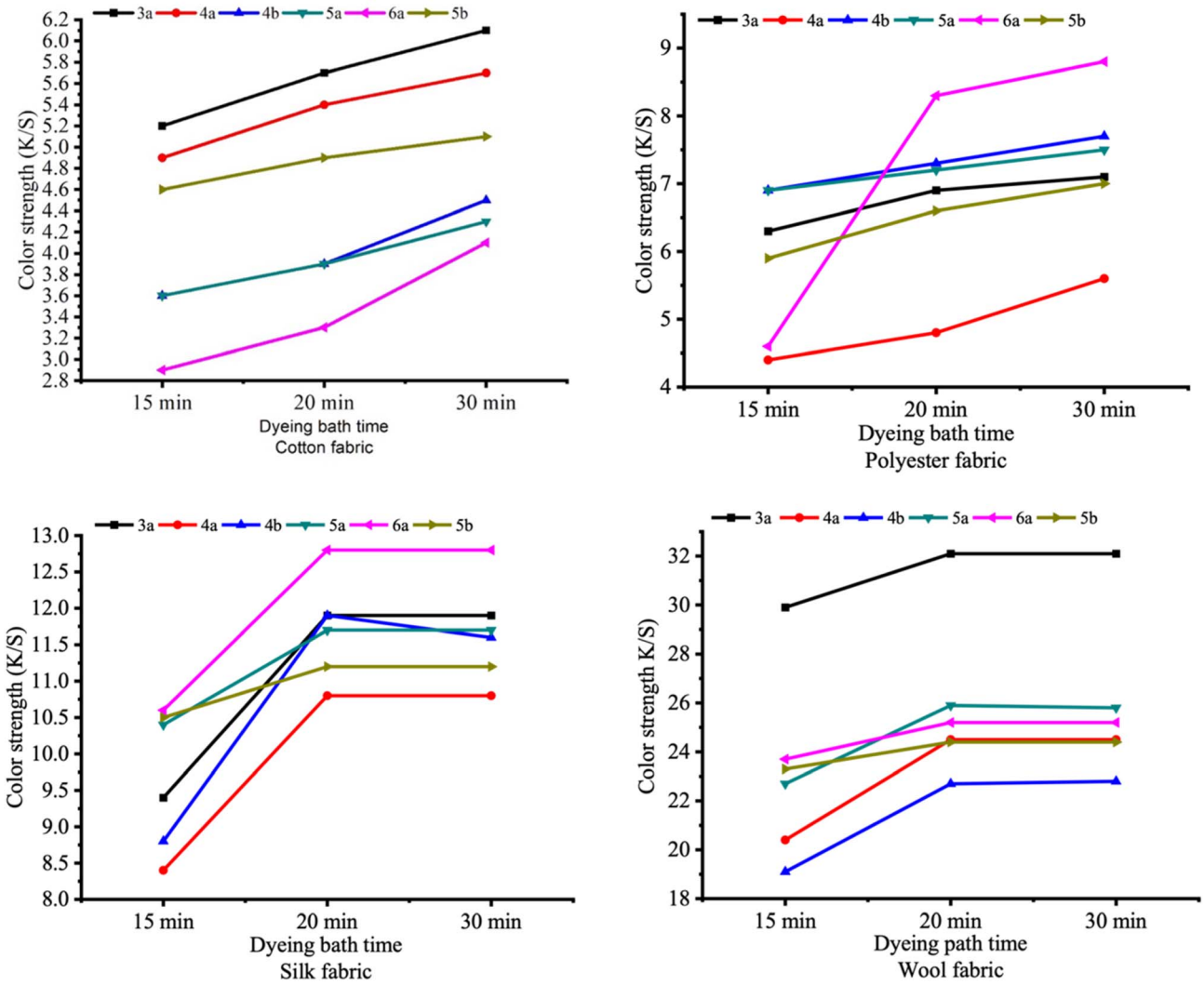

Fig. 6 The combined effect of dyeing bath time (min.) of cotton, wool, silk, and polyester fabric dyed with new synthesized dyes assisted by MW irradiation.

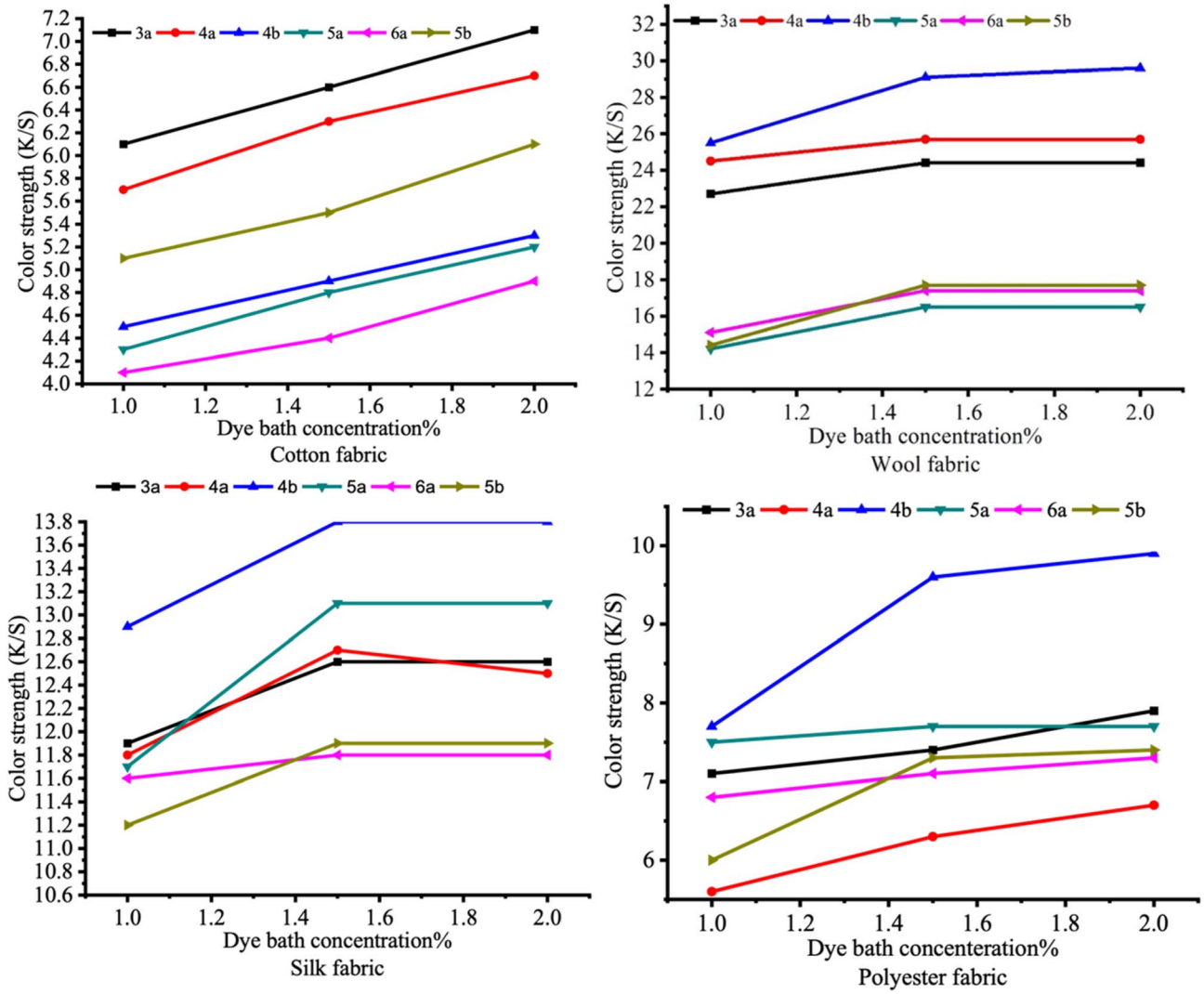

Fig. 7 The combined effect of dyeing bath concentration (g/100 mL H_2O) of cotton, wool, silk, and polyester fabric dyed with newly synthesized dyes assisted by MW irradiation.

except temperature it was carried out at 80 °C. From the data tabulated in Table 1, it was noted that IR demonstrated lower *K*/*S* values. MW irradiation plays a crucial role in enhancing the shading process. The power of microwave radiation not only facilitates the penetration of the shading agents but also determines the depth of infiltration within the fabric. This remarkable capability significantly elevates the effectiveness of microwave shading compared to traditional methods. Embrace the advantages of microwave technology for superior results.

To evaluate the statistical significance of the observed differences in color strength, a two-tailed Student's *t*-test was applied to the *K*/*S* values obtained from MW and IR dyeing methods. Although isolated dye-fiber combinations exhibited slightly higher *K*/*S* values under IR heating, the overall dataset demonstrated a statistically significant enhancement in color strength for MW-assisted dyeing ($p < 0.05$). This confirms that the improved dye uptake observed under MW irradiation is systematic and reproducible, rather than attributable to random experimental variation. The enhanced performance can be attributed to rapid volumetric heating, improved dye diffusion, and increased fiber accessibility under MW conditions.

Fastness properties

Tables 2 & 3 outlines the fastness properties of cotton, wool, silk, and polyester fabrics dyed with new synthesized dyes, specifically examining their wash-fastness, rub-fastness (wet & dry), perspiration fastness (acidic & alkaline), and light-fastness, when apply microwave irradiation and IR heating methods, respectively. The findings indicate that all dyed fabric exhibit superior wash, rub, perspiration, and light fastness, except for samples processed with IR methods. As expected, the application of microwave irradiation typically improved the color fastness characteristics, than IR heating techniques. However, rub fastness under the IR heating method demonstrated only moderate effectiveness. Furthermore, the analysis reveals that

Table 1 Effect of using different heating methods on color strength of different fabric dyed with different new synthesized dyes

	Color strength *K*/*S*			
Heating type	Cotton	Wool	Silk	Polyester
3a				
MW	7.1	33.3	13.6	7.9
IR	5.4	35.7	9.1	6.8
4a				
MW	6.7	15.5	12.7	6.7
IR	4.3	9.4	7.7	5.1
4b				
MW	5.3	14.4	12.8	8.6
IR	3.7	8.7	5.8	5.9
5a				
MWI	5.2	16.5	13.1	7.7
IR	5.3	9.4	8.7	6.8
5b				
MW	6.1	17.7	12.9	7.8
IR	3.8	12.1	9.4	3.6
6a				
MW	4.9	17.4	13.6	9.4
IR	2.2	7.6	6.4	4.7

microwave heating consistently resulted in the most advantageous color fastness properties, irrespective of whether fabric and dye were applied.

Quantitative sustainability

To quantitatively substantiate the sustainability claims, microwave-assisted dyeing was compared with conventional infrared heating in terms of energy consumption, water usage, and dye utilization efficiency. The results, summarized in Table 4, clearly demonstrate that microwave irradiation significantly reduces energy demand, processing time, and residual dye in the effluent, confirming the environmental and operational advantages of the proposed method.

Considering a cradle-to-gate life-cycle perspective, microwave-assisted dyeing significantly reduces cumulative energy demand, process water usage, and effluent dye load during the textile coloration stage, thereby lowering both upstream resource consumption and downstream wastewater treatment requirements relative to infrared-based dyeing.

Energy consumption was calculated based on applied power and effective dyeing time for both MW and IR heating methods. Water usage was determined from the applied liquor ratio, while dye fixation efficiency was calculated from the difference between initial dye concentration and residual dye concentration in the post-dyeing bath, measured spectrophotometrically. All calculations were performed per single dyeing cycle under identical fabric mass and dye concentration conditions. Residual dye concentration was determined by UV-vis analysis of the post-dyeing bath using calibration curves constructed from standard dye solutions.

Molecular docking

All the six dyes were subjected to molecular docking to test their activity as antimicrobial. Two proteins have been chosen, one for bacterial infection (*Yersinia pestis*) and the other for fungi infection (*C. albicans*). Dihydropteroate synthase in bacteria (Gram-positive or negative) is responsible for folate synthesis which is essential for nucleotide biosynthesis and amino acid metabolism in bacteria.[15,80]

The fact that bacteria have no uptake mechanism for folic acid, unlike human, makes DHPS a vital target for the synthesis of new therapeutic agents.[81] The second target is *N*-myristoyltransferase (NMT), facilitates the attachment of the fatty acid myristate from myristoyl-CoA to the N-terminal glycine residue of various proteins found in eukaryotic cells and viruses.[82] Inhibiting NMT selectively is proposed to disrupt various essential processes in the parasite by affecting multiple downstream target proteins.

The key interaction of co-crystallized inhibitor (sulfamethoxazole) with DHPS was through hydrogen bond between Ser222 and sulfonyl group of sulfamethoxazole. This interaction mimics the one with *p*ABA and Ser222 which results in inhibition. Additionally, Lys221, Phe28, and Pro64 were included in the interaction with inhibitor. All the dyes showed more stable interaction compared to original ligand (−5.76) with binding affinities ranged from −5.88 to −6.95 kcal mol^{-1} and RMSD

Table 2 Fastness characteristics associated with the concurrent dyeing of fabrics samples using synthesized dye facilitated by MW irradiation

	Washing fastness		Rubbing fastness		Perspiration fastness				
					Acidic		Alkaline		
Dyed fabrics	Alt	Stain	Dry	Wet	Alt	Stain	Alt	Stain	Light fastness
3a									
Cotton	3	3	4	3–4	4	4–5	4	4	6
Wool	4–5	4	4–5	4–5	4–5	4–5	4–5	4–5	6–7
Silk	4–5	4–5	4–5	4–5	4–5	4–5	4–5	4–5	6–7
Polyester	4	4	4	3–4	3–4	3–4	4	4	6
4a									
Cotton	3	3	3	3	3	4	4	4–5	6
Wool	4–5	4–5	4–5	4	4	4–5	4–5	4–5	6–7
Silk	4	4	4–5	4–5	4–5	4–5	4	4	6–7
Polyester	3	3	3	3	3	3	4	4	5–6
4b									
Cotton	4	4	3–4	3–4	3	3	3	4	5–6
Wool	4	4–5	4–5	4	4	4–5	4–5	4–5	6–7
Silk	4	4	4–5	4–5	4–5	4–5	4	4	6–7
Polyester	4	4	3–4	3–4	3–4	3–4	4	4	6
5a									
Cotton	3–4	3–4	3–4	3–4	3–4	3–4	4	4	6
Wool	4–5	4–5	4–5	4–5	4–5	4–5	4	4	6–7
Silk	4–5	4	4	4	4	4–5	4–5	4–5	6–7
Polyester	3–4	3–4	3–4	3–4	3	3	3	3–4	5–6
5b									
Cotton	3	3	3–4	3–4	3–4	3	3	3	5–6
Wool	3–4	4	4	4	4–5	4–5	3–4	4	6–7
Silk	4	4	4	4–5	4–5	4–5	4–5	4–5	6–7
Polyester	3	4	4	3	3–4	3–4	3–4	3–4	6
6a									
Cotton	3	3	3	3–4	3–4	4	4	3–4	5–6
Wool	4–5	4–5	4–5	4–5	4–5	4–5	4–5	4	6–7
Silk	3–4	4	4–5	4–5	4–5	4–5	4	4	6–7
Polyester	3–4	3–4	3	3	3	3	3	3	5–6

values less than 1.7 Å (Fig. 8). Compounds **4a**, **4b**, and **5a** have similar interaction with original ligand at Ser222 (Table 5).

Since prepared dyes are relatively large molecules and according to the previous results of docking, the dyes interacted with two residues Lys221, and Arg255, which are common sites at Pterin and *p*ABA,[83] a second docking study performed to test these dyes as possible dual inhibitors. The docking performed in the same pocket of the same PDB structure at the same settings, the only difference was performing the docking at sulfamethoxazole and Pterin atoms. The binding affinity of all dyes increased because of the additional stabilized interactions formed at the key residues of both *p*ABA and Pterin such as Ser222, Asp96, and Arg255 which resembles the ones with original ligands (Table 6). However, **4b** and **6a** have binding affinity lower compared to docking at sulfamethoxazole only.

The important residues in interaction with NMT are Tyr225, Tyr354, Phe117, and Phe339. However, the co-crystallized inhibitor formed stable interaction with Leu451, Tyr119, His227, and Asn392 which also acceptable binding sites.[84] The docked dyes showed similar interactions with Leu451. The binding affinity ranged from −7.23 to −8.179 kcal mol^{-1} which are like original ligand binding affinity (−8.179 kcal mol^{-1}) (Fig. 9). We can conclude that they have promising antifungal and antibacterial properties (Table 7).

Antibacterial property

The antimicrobial efficacy of synthesized dyes was influenced by its chemical composition and the specific functional groups it contained, as well as the functional group presented in dyed fabrics. Consequently, an investigation was conducted into the antimicrobial qualities of these dyed fabrics with respect to *S. aureus* (Gram-positive bacteria), *K. pneumoniae* (Gram-negative bacteria), and *C. albicans* (fungus). This analysis utilized the optical density method, and the resulting data have been compiled in Table 8.

On fabric

The study reveals that antimicrobial effectiveness is markedly higher against bacteria compared to fungi, with a more

Table 3 Fastness characteristics associated with the concurrent dyeing of fabrics samples using synthesized dye facilitated by IR heating method

	Washing fastness		Rubbing fastness		Perspiration fastness				
					Acidic		Alkaline		
Dyed fabrics	Alt	Stain	Dry	Wet	Alt	Stain	Alt	Stain	Light fastness
3a									
Cotton	2–3	2–3	3	2–3	2	2	2–3	3	5–6
Wool	2–3	3	3	3	2–3	2–3	2–3	2–3	6
Silk	4–5	4–5	4–5	4–5	4–5	4–5	4–5	4–5	6
Polyester	4	4	4	3–4	3–4	3–4	4	4	5–6
4a									
Cotton	3	3	3	3	3	4	4	4–5	5
Wool	4–5	4–5	4–5	4	4	4–5	4–5	4–5	5–6
Silk	4	4	4–5	4–5	4–5	4–5	4	4	5–6
Polyester	2–3	2–3	2–3	2	2	3	2–3	2–3	5
4b									
Cotton	2	2	3	3	2–3	2	2–3	2–3	4–5
Wool	3	3	3	2	2–3	2–3	2–3	3	5
Silk	4	4	4–5	4–5	4–5	4–5	4	4	5
Polyester	4	4	3–4	3–4	3–4	3–4	4	4	4–5
5a									
Cotton	3	3	3	2	2–3	2–3	2–3	2–3	4–5
Wool	4	4	4	3	3	3	3	2–3	5
Silk	3	3	3	3	2–3	2–3	2–3	2–3	5
Polyester	2	2	2–3	2–3	2–3	2–3	2–3	2–3	3–4
5b									
Cotton	2	2	3	2–3	3–4	2–3	2–3	2–3	4–5
Wool	3	3	3	3	3	3	2–3	2–3	5
Silk	3	3	3	2–3	2–3	2–3	2–3	2–3	5
Polyester	2	2–3	2–3	2–3	2–3	2–3	3	3	3–4
6a									
Cotton	2–3	2–3	2–3	2–3	2–3	3	3	3	4
Wool	4–5	4–5	4–5	4–5	4–5	4–5	4–5	4	4–5
Silk	3–4	4	4–5	4–5	4–5	4–5	4	4	4–5
Polyester	3–4	3–4	3	3	3	3	3	3	4

significant reduction observed in the Gram-positive bacterium *S. aureus* than in the Gram-negative bacterium *K. pneumoniae*. This discrepancy can likely be traced to the inherent structural differences between bacteria and fungi. Among the various heating methods analyzed, microwave heating demonstrated superior antimicrobial reduction capabilities. The data tabulated in Table 8 indicate that: (i) total bacteria account% value is higher when applying microwave irradiation than IR heating

Table 4 Quantitative sustainability comparison between MW and IR dyeing methods

Parameter	Microwave dyeing (MW)	Infrared dyeing (IR)	Sustainability advantage
Heating power (W)	70–90 W	500–600 W	MW uses lower applied power
Dyeing time (min)	10–15	45–60	~4–5× reduction in process time
Total energy consumption/cycle (kJ)[a]	42–81	1350–2160	~90–95% energy saving
Dye bath temperature (°C)	65–92	95–100	Lower thermal stress in MW
Water volume per batch (L)	0.05	0.10	~50% water saving
Dye fixation (%)	85–92	70–78	Higher fixation efficiency
Residual unfixed dye in bath (%)	8–15	22–30	Reduced effluent load
Need for auxiliary chemicals	Reduced	Conventional	Lower chemical demand
Overall environmental impact	Low	Moderate–High	MW is more sustainable

[a] Energy consumption calculated as: energy (kJ) = power (kW) × time (s).

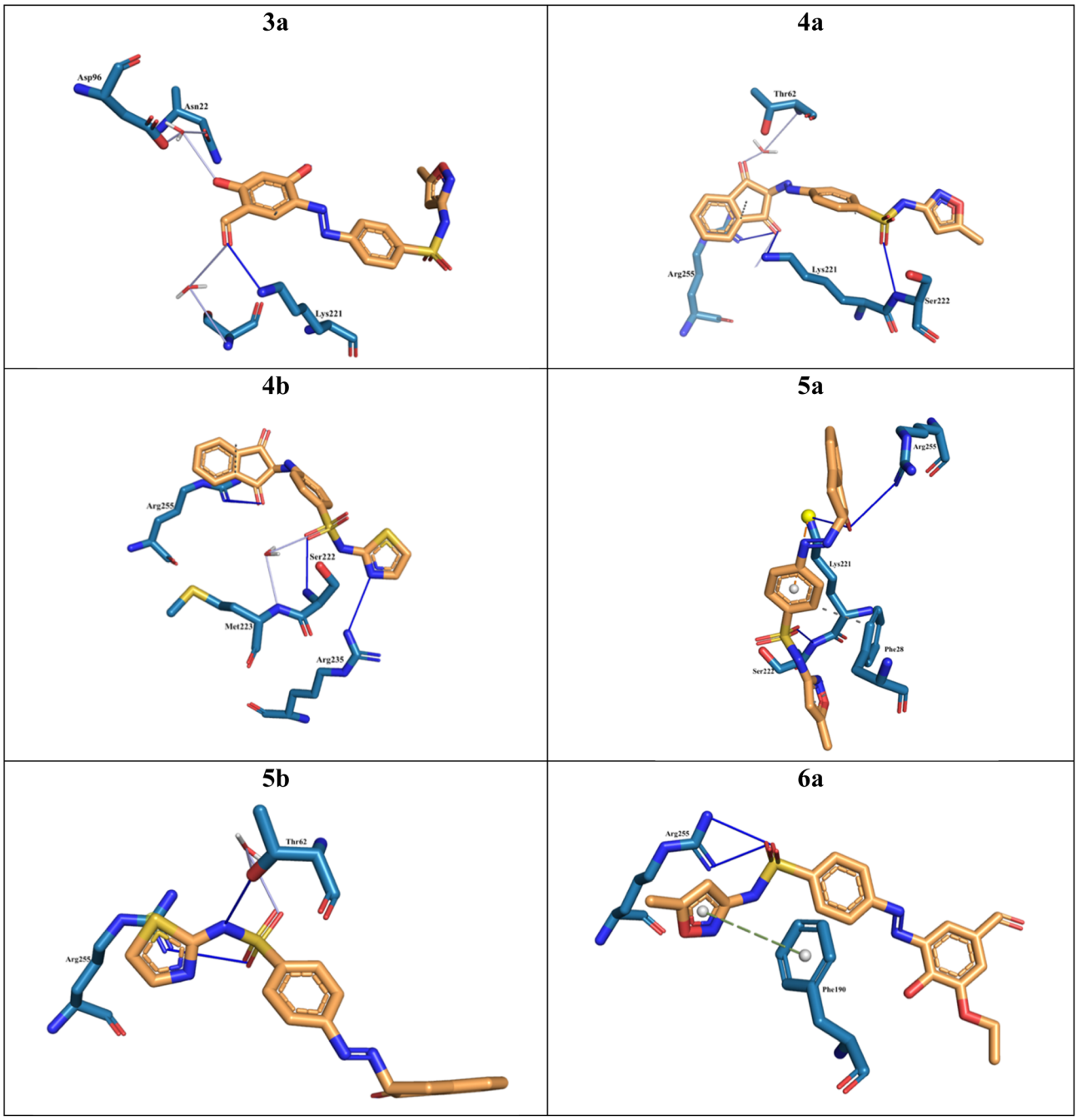

Fig. 8 Illustration of main residues incorporated in the interaction of dyes.

method, (ii) *S. aureus* (G+) gave a higher value than *K. pneumoniae* (G−) and *C. albicans* (Fungi) when applying microwave heating, while when applying IR heating method the *K. pneumoniae* (G−) gave a higher reduction value than *S. aureus* (G+) and *C. albicans* (Fungi), (iii) synthesized dye namely **4b** gave a higher value than the other dyes under study, (iv) wool fabric has a higher value for all total bacterial and fungal count%, while polyester fabric gave the lowest value.

Although molecular docking studies predicted strong binding affinity of the synthesized dyes toward fungal *N*-myristoyltransferase (NMT), the antifungal performance observed for the dyed fabrics against *C. albicans* was comparatively limited. This apparent discrepancy can be rationalized by considering the physicochemical constraints imposed by the fiber matrix. In the fabric-based assay, bioactivity depends not only on the intrinsic molecular affinity of the dye but also on its mobility, diffusion, and release from the fiber surface. The strong fixation of the sulfa-azo dyes within the textile matrix, which is advantageous for color fastness and environmental sustainability, simultaneously restricts dye leaching into the surrounding medium, thereby limiting direct contact with fungal cells. Consequently, the reduced antifungal efficacy

Table 5 Binding affinity scores for each dye and type of bonds formed with *p*ABA pocket residue[a]

Compound	BA (kcal mol^{-1})	RMSD (Å)	Binding residue
3a	−6.186	1.4	Lys221 (H-bond donor to oxygen of aldehyde group) Oxygen of hydroxyl bonded by hydrogen bond with water molecule
4a	−6.184	1.5	Ser222 (backbone acceptor to oxygen of sulfonyl group similar interaction of *p*ABA) Oxygen of indandione forms water bridge with Arg255
4b	−6.95	1.6	Ser222 (backbone acceptor to oxygen of sulfonyl group similar interaction of *p*ABA) Arg235 is hydrogen-bonded to *N*-imide of thiazole ring Oxygen of indandione forms water bridge with Arg 255 Oxygen of sulfonyl forms water bridge with Met223
5a	−6.83	1.2	Ser222 (backbone acceptor to oxygen of sulfonyl group similar interaction of *p*ABA) Lys221 is hydrophobic/π stacking interaction to benzene ring of sulfa dye Arg63 is hydrophobic/π stacking interactions to benzene ring of sulfa dye Phe 28 is hydrophobic bonded to hydrogen atom of benzene ring of sulfa dye Oxygen of indandione forms water bridge with Arg 255
5b	−5.88	1.57	Arg255 H-bond donor to oxygen of sulfonyl and at the same time forms water bridge with sulfonyl group Asp 96 is H-bond acceptor from sulfur of thiazole ring water molecule is H-bond attached to oxygen of sulfonyl
6a	−6.48	1.5	Arg255 is H-bond donor to oxygen of sulfonyl group Hydrophobic interaction from Arg255 and Phe190 to oxazole 5-membered ring

[a] BA: binding affinity RMSD: root-mean square deviation.

observed on fabrics reflects controlled dye immobilization rather than a lack of molecular bioactivity. This distinction highlights the fundamental difference between *in silico* molecular predictions and solid-state, application-based antimicrobial evaluations.

Theoretical investigation

Density functional theory (DFT) is a super-efficient, fundamental computer method used to figure out the basic, or "ground-state" characteristics of a molecule. It's become a top choice because it can predict a molecule's electronic behavior very accurately and much faster than many older computational techniques. Essentially, it is a powerful shortcut for chemical prediction.[85]

Optimized structures

The image displays the optimized molecular structures of six compounds (Fig. 10), labeled **3a**, **4a**, **4b**, **5a**, **5b**, and **6a**, these optimized geometries are crucial for predicting the compounds' physical, electronic, and functional properties due to the

Table 6 Binding affinity scores for each dye and type of bonds formed with *p*ABA and Pterin pocket residue[a]

Compound	BA (kcal mol^{-1})	RMSD (Å)	Difference in binding residue
3a	−6.6102	1.36	Ser222 (backbone acceptor to two oxygens of sulfonyl group similar interaction of *p*ABA) Asp96 is H-bond acceptor from OH of 2,4-dihydroxybenzaldehyde (Pterin residue) Lys221 didn't interact
4a	−6.4999	1.86	Ser222 (backbone acceptor to oxygen of sulfonyl group similar interaction of *p*ABA) Oxygen of indandione forms water bridge with Arg255
4b	−6.77	1.54	Lys221 pi stacking interaction with benzene ring of sulfamethoxazole (Pterin/*p*ABA residue) Arg235 didn't interact with dye
5a	−6.90	1.84	Oxygen of sulfonyl forms water bridge with Met223 NH of sulfamethoxazole forms water bridge with Gly189 Lys221, Phe25, Arg63 didn't interact
5b	−6.49	1.66	Ser222 (pi stacking to thiazole ring) Oxygen of sulfonyl forms water bridge with Met223 Asp 96 is backbone acceptor from indandione H atom Arg255 didn't interact
6a	−6.267	1.7	Hydrophobic interaction from Arg255 only to oxazole 5-membered ring

[a] BA: binding affinity RMSD: root-mean square deviation.

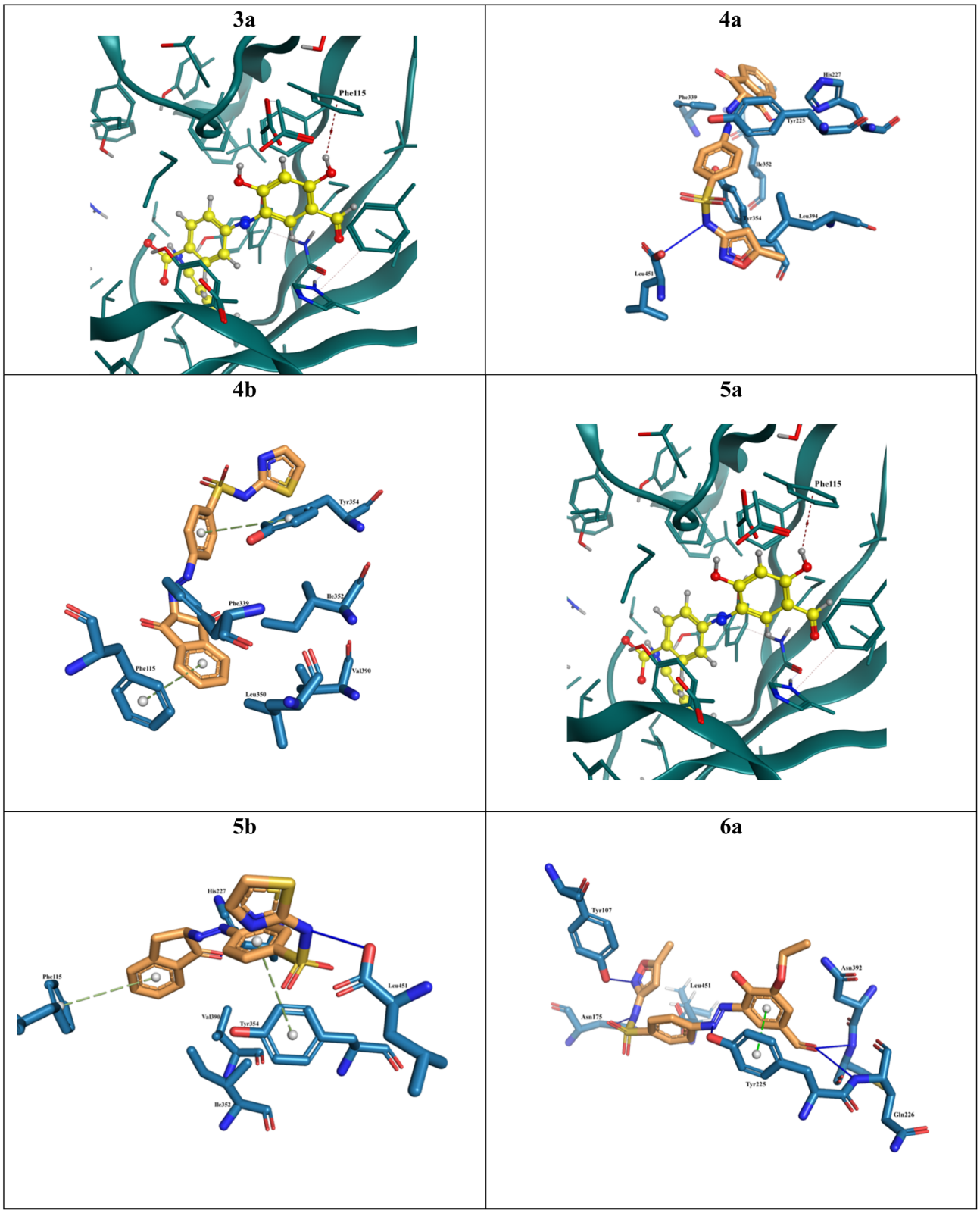

Fig. 9 Illustration of main residues incorporated in the interaction of dyes.

presence of common functional groups (–SO_2NH– and –N=N–). The optimized structures universally show an *E* (or *trans*) configuration about the N=N double bond.[86] This isomer is almost always the more stable form due to less steric hindrance between the attached groups and the ability to maximize the conjugation across the entire molecule, leading to a more planar and energetically favorable geometry. Also, the relatively planar arrangement of the Ar–N=N–Ar core in most structures

Table 7 Binding affinity scores for each dye and type of bonds formed with NMT pocket residue

Compound	BA	RMSD	Binding residue
3a	−8.021	1.38	Phe115 hydrophobic interaction with OH of 2,4-dihydroxybenzaldehyde
4a	−8.179	1.59	Leu451 forms H-bond with NH of sulfamethoxazole
4b	−7.288	1.2	Tyr354 forms hydrophilic-pi stacking interaction with benzene ring and thiazole ring Phe115 forms hydrophobic–H interaction with H of benzene ring of indandione
5a	−7.934	1.57	Tyr354 forms hydrophilic-pi stacking interaction with oxazole ring
5b	−7.23	1.09	Leu451 acts as H-bond acceptor from NH and S of sulfathiazole Tyrs354 hydrophilic-pi stacking interaction with benzene ring of sulfamethoxazole
6a	−7.145	1.69	Leu451 backbone acceptor from H of benzene of sulfamethoxazole part Tyr225 pi-stacking with benzene ring of vanillin Gln226 H-bond with aldehydic oxygen of vanillin Asn175 backbone acceptor from NH of sulfamethoxazole part Tyr107, pi-stacking with methoxazole ring

Table 8 The antibacterial properties of different fabrics that have been dyed using new synthesized dyes, employing various heating techniques in the process

	Total bacteria count (*R*%)		Total fungal count (*R*%)	Total bacteria count (*R*%)		Total fungal count (*R*%)
	S. aureus (G+)	*K. pneumoniae* (G−)	*C. albicans* (Fungi)	*S. aureus* (G+)	*K. pneumoniae* (G−)	*C. albicans* (Fungi)
	Reduction (%)	Reduction (%)	Reduction (%)	Reduction (%)	Reduction (%)	Reduction (%)
Fabrics	Microwave irradiation			IR heating		
3a						
Cotton	23	18	14	17	19	10
Wool	71	65	38	22	48	26
Silk	68	58	31	18	34	17
Polyester	28	23	16	21	24	19
4a						
Cotton	19	16	11	15	13	9
Wool	66	56	22	17	22	15
Silk	53	44	21	11	17	14
Polyester	20	18	13	18	20	17
4b						
Cotton	38	32	23	26	31	16
Wool	89	78	42	33	42	34
Silk	82	70	38	26	31	24
Polyester	29	35	26	20	24	21
5a						
Cotton	31	25	16	19	24	9
Wool	77	69	35	27	34	22
Silk	75	62	30	20	25	17
Polyester	22	28	19	16	18	12
5b						
Cotton	28	24	20	20	23	13
Wool	75	71	32	27	31	24
Silk	67	51	28	31	38	24
Polyester	22	16	14	17	19	12
6a						
Cotton	26	23	15	17	19	15
Wool	71	63	29	21	25	17
Silk	64	55	26	22	27	19
Polyester	19	15	13	15	18	11

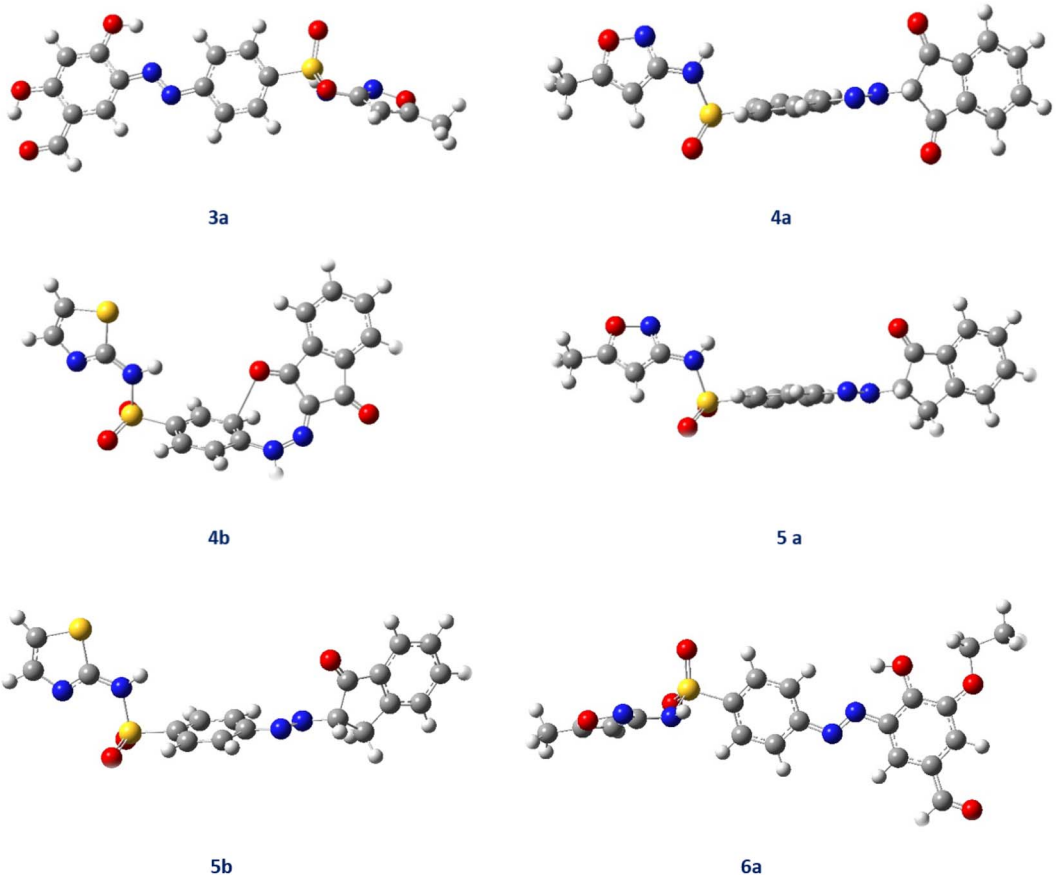

Fig. 10 Optimized and chemical structure of newly synthesized dyes **3–6**(a–b).

confirms the maximum conjugation, which directly relates to the energy of the electronic transitions ($\pi \rightarrow \pi^*$) and, consequently, the color of the synthesized dyes. Structures like **3a**, **4a**, **5a** and **5b** that appear capable of intramolecular hydrogen bonding (*e.g.*, O–H···N or N–H···O) are expected to be more stable, particularly against solvent effects.[87] The bond rotations around the Ar–S and S–N bonds, visible in **4b**, **5a**, and **5b**, indicate minimized steric clash in the optimized structures. The degree of this twist can impact on the overall conjugation and thus the final color.

Analysis of frontier molecular orbitals (FMOs)

The HOMO and LUMO are the orbitals involved in the lowest-energy electronic transition (HOMO → LUMO), which is responsible for the molecule's absorption of visible light and, thus, its color. Table 9 and Fig. 11 represent HOMO (donor): the HOMO (typically the red/pink lobes) is generally localized over the sulfonamide-substituted aromatic ring (the diazo component) and the N=N bridge. This suggests that the sulfonamide group, particularly its $-SO_2NH$ substituent, is the electron-

Table 9 Physicochemical data for new synthexsized dyes **3–6**(a/b)

	Compounds					
Physicochemical parameters	**3a**	**4a**	**4b**	**5a**	**5b**	**6a**
E_{LUMO}	−3.4994	−3.0798	−3.0398	−2.8520	−2.8545	−2.206
E_{HOMO}	−6.8711	−6.9117	−6.1938	−6.6880	−6.1925	−5.4933
ΔE	3.3718	3.8319	3.1541	3.8360	3.3380	3.2873
χ	5.1853	4.9957	4.6168	4.7700	4.5235	3.8497
η	1.6859	1.9159	1.5770	1.9180	1.6690	1.6437
σ	0.5932	0.5219	0.6341	0.5214	0.5992	0.6084
Pi	−5.1853	−4.9957	−4.6168	−4.7700	−4.5235	−3.8497
S	0.2966	0.2610	0.3171	0.2607	0.2996	0.3042
Ω	7.9741	6.5130	6.7579	5.9314	6.1299	4.5082
ΔN_{max}	3.0757	2.6074	2.9275	2.4870	2.7103	2.3421
Dipole moment	3.3057	7.4501	6.7374	7.3288	8.7365	1.5676
Electronic energy	−1724.0586	−1725.0376	−2008.7389	−1651.0592	−1934.7450	−1802.6392

donating group (EDG) in this system. LUMO (acceptor): the LUMO (typically the green lobes) is consistently localized over the coupled aromatic ring and its substituents (the coupling component). This is the electron-withdrawing region (EWG). The HOMO–LUMO energy gap (ΔE) is inversely proportional to the maximum absorption wavelength (λ_{max}).[88]

A smaller ΔE requires less energy, corresponds to a longer λ_{max} (bathochromic shift), and usually results in a color shift toward red or blue. Compound **4b** (ΔE = 3.154 eV) shows the smallest energy gap, due to the presence of the thiazole ring which is a strong electron-withdrawing group (EWG) when attached to the SO_2 group, enhancing the electron-donating power of the nitrogen atom in the sulfonamide and effectively reducing the overall energy gap. Compounds **4a** and **5a** showed the highest ΔE ($\Delta E \approx$ 3.83 eV), suggesting they absorb at the shortest wavelength and likely be yellow or orange (least bathochromic shift). Compounds **4a** and **5a** feature methoxazole substituent on the sulfonamide nitrogen, which is a weaker electron-donating group compared to the thiazole group in **4b** and **5b**. It means that oxazole derivatives have less aromatic character than thiazole.

Less aromaticity means the -electrons are less effectively delocalized over the ring, making the ring less stable and more reactive, and often exhibiting a stronger net electron-

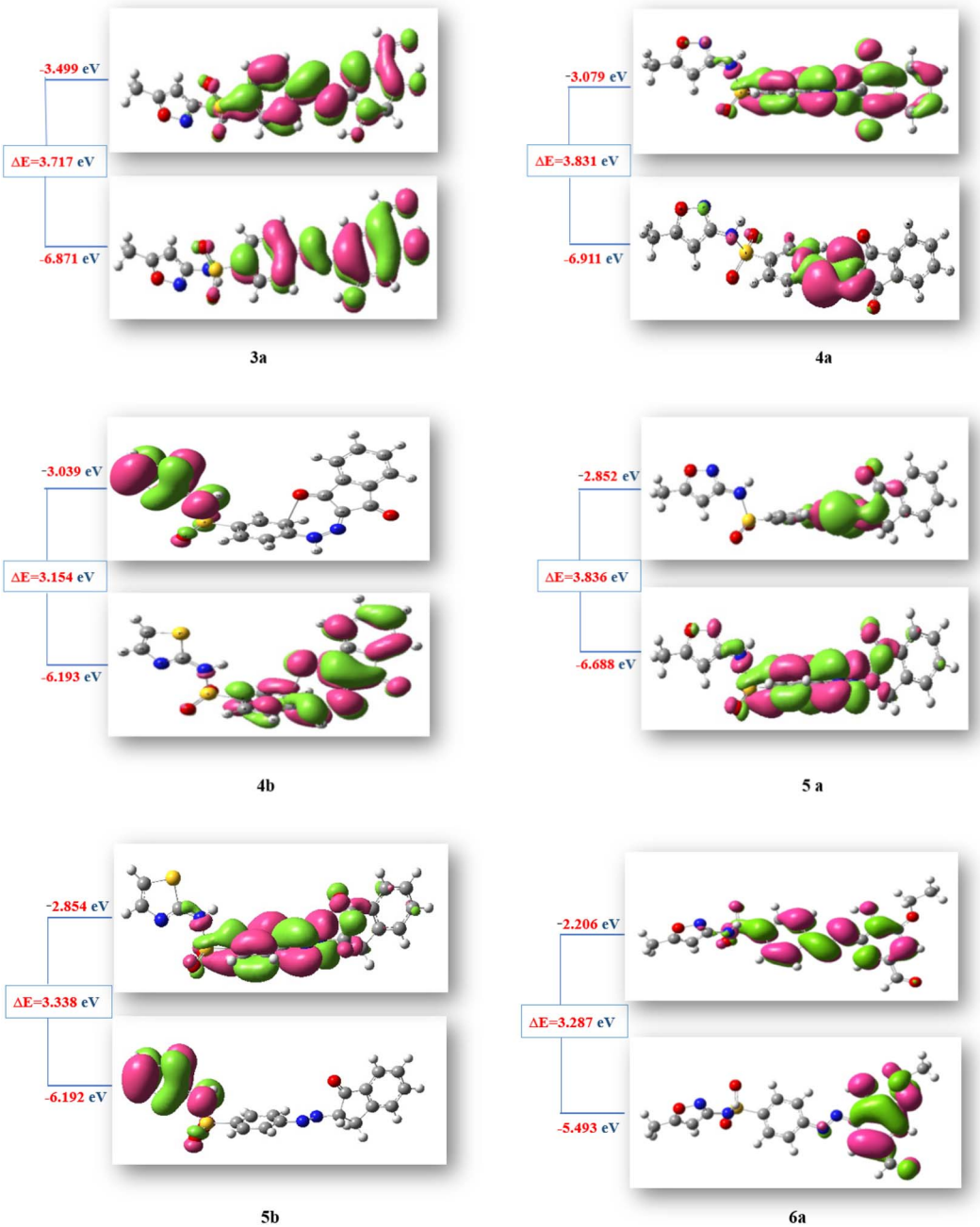

Fig. 11 HOMO and LUMO energy gap of new synthesized dyes **3–6**(a–b).

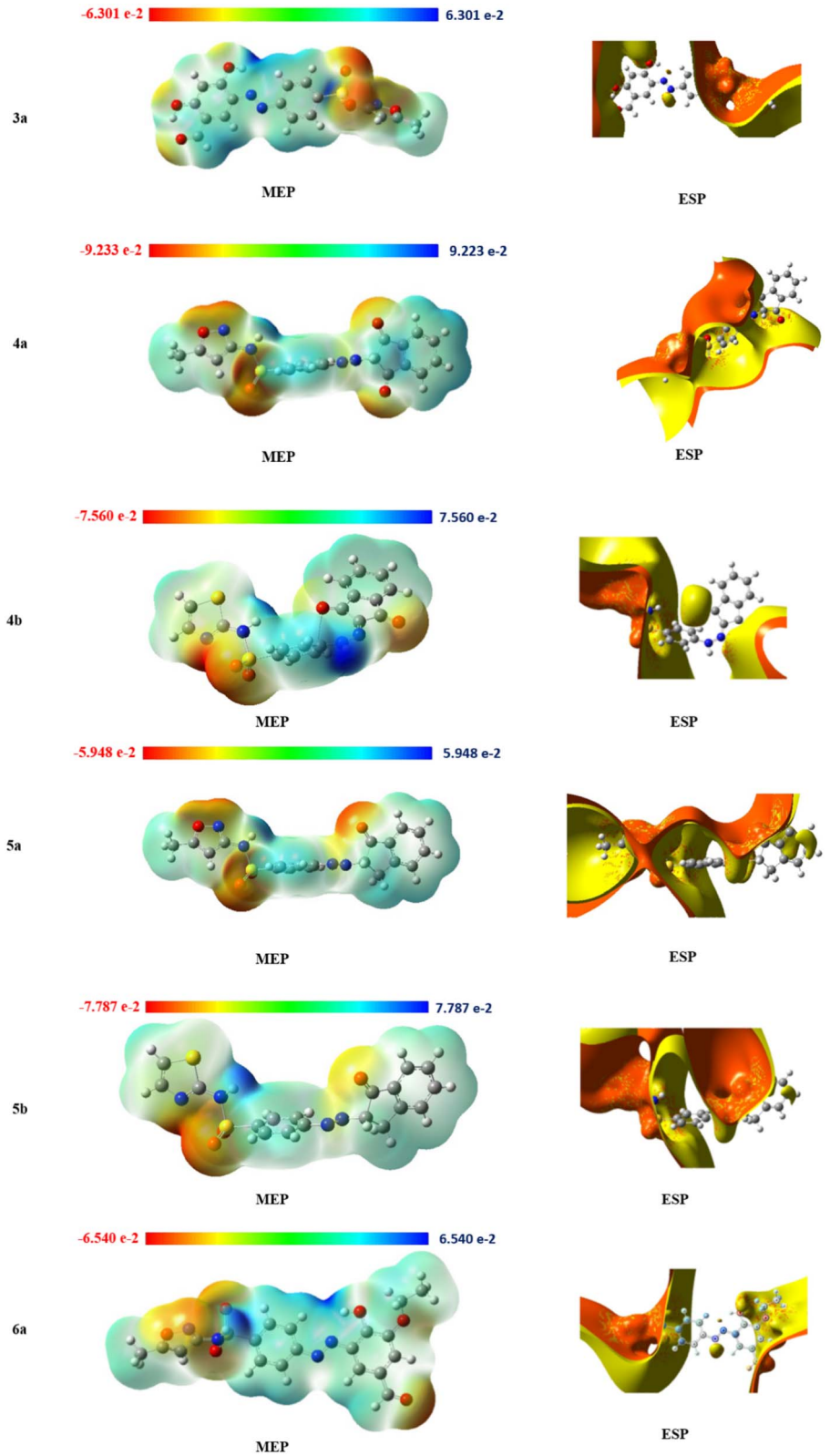

Fig. 12 MEP and ESP isosurfaces of newly synthesized dyes 3–6(a–b).

withdrawing effect. The weaker donation results in a less stable (lower energy) HOMO and a larger ΔE. The dipole moment is a measure of molecular polarity. The values are relatively high, ranging from 3.0057 to 8.7365 debye, indicating that these dye molecules are significantly polar, which would impact their solubility and interaction with substrates.[89]

The energy values of HOMO and LUMO energy levels, which were calculated using the DFT/B3LYP6-3G(d) computational method, are used to derive a variety of other significant chemical parameters that quantify the molecules' intrinsic properties. These derived parameters, which include the absolute electronegativity (χ), the chemical potential (Pi), the absolute hardness (η), the absolute softness (σ), the global electrophilicity (ω), and the global softness (S), are all tabulated in Table 9 and were determined by applying a set of specific governing equations.[90–94]

The synthesized azo dyes resistance to changes in electron distribution is quantified by their chemical hardness (η) and softness (σ). The hardness values range narrowly from 1.6859 to 1.9159 eV, and the corresponding softness values are between 0.5219 and 0.5992 eV. Notably, higher hardness (η) suggests greater stability and, consequently, lower reactivity for the molecule. Additionally, the electronegativity (χ), which measures the tendency of an atom or molecule to attract electrons, shows values ranging from 4.5235 eV to 5.1853 eV. The electrophilicity index (ω), which reflects the energy stabilization gained when a molecule accepts an electronic charge, exhibits consistently high values (from 5.9314 to 7.9741), strongly indicating that these compounds function as strong electrophiles (electron-seeking species). This electrophilic nature is further supported by the relatively high values of the maximum charge transfer (ΔN_{max}), which falls between 2.3421 and 3.0757 and represents the total electronic charge the electrophile can accept.[95]

Mapping and molecular parameters

The molecular electrostatic potential (MEP) and electrostatic potential (ESP) maps provide a visual representation of the charge distribution and electronic potential around the molecules, which is crucial for predicting their intermolecular interactions and sites of chemical reactivity.

The MEP surfaces for the synthesized sulfa-azo dyes (**3a** to **6a**/b) use a color-coded map to visually represent the charge distribution and potential reactivity of the molecules: red regions denote areas of most negative potential (highest electron density), making them the most favorable sites for electrophilic attack or H-bond donor interactions; conversely, blue regions signify areas of most positive potential (electron-deficient), identifying them as the most likely sites for nucleophilic attack or H-bond acceptor interactions, while green areas represent the neutral or near-zero potential regions. The MEP analysis of the sulfa-azo dyes consistently shows the sulfonamide S═O oxygens and azo N═N nitrogens as the most electron-rich sites (intense red), making them the primary targets for electrophilic attack or H-bond acceptance; this is also seen on the phenolic O–H oxygens of compound **3a**. Conversely, the most significant blue regions (electron-deficient) are localized on the protons of the sulfonamide –NH and hydroxyl –OH groups as in **3a** and **6a**, confirming their role as H-bond donors.

This overall MEP distribution reflects the sulfa-azo moiety's nature as a strong electron-donating group (EDG) toward the coupled aromatic ring. This polarizing effect is particularly strong in compounds **3a** and **6a**, which contain strong EDG/EWG (–OH/–CHO), leading to a highly polarized molecular surface, high dipole moments (see Fig. 12), and the most intense color differentiation on the MEP scale.[95]

ESP visualizations confirm the large separation of charge across the molecule (consistent with the large, calculated dipole moments in Table 9), with a highly negative region dominating the sulfa-azo portion and the H-bond acceptor sites, and a positive region (often shown as yellow/green) near the N–H and O–H protons. This clear spatial separation of positive and negative potential is characteristic of highly polar push–pull electronic systems, which are typical for azo dyes. This charge separation is responsible for the observed electronic properties, including the color of the compounds and their ability to interact strongly with polar solvents or substrates during the dyeing process.[86]

Correlation of ESP results with optical properties and dye–fiber interactions of 4b

The ESP and MEP surfaces of compound **4b** (Fig. 12) reveal a pronounced heterogeneous charge distribution across the molecular framework. Strong negative potential regions (red–orange, down to -7.56×10^{-2} a.u.) are predominantly localized around the heteroatom-containing moieties, particularly the sulfonyl oxygen atoms and the nitrogen atoms within the heterocyclic and azo-linked segments. These electron-rich sites are favorable for hydrogen bonding and electrostatic interactions with protonated or electrophilic functional groups present on the fiber surface. In contrast, positive potential regions (blue, up to $+7.56 \times 10^{-2}$ a.u.) are mainly distributed over the aromatic and alkyl-substituted regions, indicating electron-deficient areas that can participate in complementary electrostatic attractions with negatively charged fiber sites. This distinct separation of electron-rich and electron-poor regions, combined with the high molecular dipole moment of **4b**, supports strong dye–fiber interactions and rationalizes the dyeing mechanism proposed. The ESP distribution thus provides a clear theoretical explanation for the enhanced fiber affinity and color strength observed experimentally for compound **4b**.[96,97]

Conflicts of interest

The authors declare no conflict of interest.

Data availability

All data generated or analyzed during this study are included in this published article and its supplementary information (SI) files. Supplementary information is available. See DOI: https://doi.org/10.1039/d5ra09499b.

References

1 N. M. Aljamali and H. S. Hassen, Review on Azo-Compounds and Their Applications, *J. Catal. Catal.*, 2021, **8**(2), 8–16, DOI: 10.37591/JoCC.
2 S. Benkhaya, S. El Harfi and A. El Harfi, Classifications, properties and applications of textile dyes: A review, *Appl. J. Envir. Eng. Sci.*, 2017, **3**(3), 311–320.
3 M. Berradi, *et al.*, *Textile Finishing Dyes and Their Impact on Aquatic Environs*, Elsevier Ltd, 2019, DOI: 10.1016/j.heliyon.2019.e02711.
4 Y. Doruk ARACAGÖK and N. CİHANGİR, Decolorization of Reactive Black 5 by Yarrowia lipolytica NBRC 1658, *Am. J. Microbiol. Res.*, 2013, **1**(2), 16–20, DOI: 10.12691/ajmr-1-2-1.
5 H. E. Gaffer, *Antimicrobial Sulphonamide Azo Dyes*, Blackwell Publishing Ltd, 2019, DOI: 10.1111/cote.12437.
6 N. M. Mallikarjuna and J. Keshavayya, Synthesis, spectroscopic characterization and pharmacological studies on novel sulfamethaxazole based azo dyes, *J. King Saud Univ., Sci.*, 2020, **32**(1), 251–259, DOI: 10.1016/j.jksus.2018.04.033.
7 A. Ovung and J. Bhattacharyya, Sulfonamide drugs: structure, antibacterial property, toxicity, and biophysical interactions, *Biophys. Rev.*, 2021, **13**, 259–272, DOI: 10.1007/s12551-021-00795-9/published.
8 J. V. Metzger, Thiazoles and their Benzo Derivatives, in *Comprehensive Heterocyclic Chemistry*, ed. A. R. Katritzky and C. W. Rees, 1984, vol. 6, ch. 4.19, pp. 235–331.
9 K. T. Chung, Azo dyes and human health: a review, *J. Environ. Sci. Health, Part C:Environ. Carcinog. Ecotoxicol. Rev.*, 2016, **34**(4), 233–261, DOI: 10.1080/10590501.2016.1236602.
10 H. Sharifi, Synthetic Medicinal Chemistry: Advancing Drug Discovery and Development, 2023, **6**, 3, 72–75, DOI: 10.37532/jmoc.
11 Y. Z. Shi, *et al.*, Sculpting nanoparticle dynamics for single-bacteria-level screening and direct binding-efficiency measurement., *Nat. Commun.*, 2018, **10**, 1227, DOI: 10.1038/s41467-019-09171-4.
12 C. Capasso; C. T. Supuran, From Molecules to Man, in *Bacterial Resistance to Antibiotics – from Molecules to Man*, Wiley, 2019, pp. 163–172, DOI: 10.1002/9781119593522.fmatter.
13 J. Qi, *et al.*, Synthesis of bi-substrate state mimics of dihydropteroate synthase as potential inhibitors and molecular probes, *Bioorg. Med. Chem.*, 2011, **19**(3), 1298–1305, DOI: 10.1016/j.bmc.2010.12.003.
14 R. Vivas, A. A. T. Barbosa, S. S. Dolabela and S. Jain, Multidrug-Resistant Bacteria and Alternative Methods to Control Them: An Overview, *Microb. Drug Resist.*, 2019, **25**(6), 890–908, DOI: 10.1089/mdr.2018.0319.
15 D. I. Hammoudeh, Y. Zhao, S. W. White, and R. E. Lee, "Replacing sulfa drugs with novel DHPS inhibitors," 2013. doi: DOI: 10.4155/fmc.13.97.
16 H. Ebiike, Design and Synthesis of Novel Benzofurans as a New Class of Antifungal Agents Targeting Fungal *N*-Myristoyltransferase, part 2, *Bioorg. Med. Chem. Lett.*, 2002, **12**(4), 607–610, DOI: 10.1016/s0960-894x(01)00808-3.
17 M. D. Resh, *Trafficking and Signaling by Fatty-Acylated and Prenylated Proteins*, Nature Publishing Group, 2006, DOI: 10.1038/nchembio834.
18 S. Ghomashi, *et al.*, Evaluation of antibacterial, cytotoxicity, and apoptosis activity of novel chromene-sulfonamide hybrids synthesized under solvent-free conditions and 3D-QSAR modeling studies, *Sci. Rep.*, 2024, **14**, 12878, DOI: 10.1038/s41598-024-63535-5.
19 S. S. Swain, S. K. Paidesetty and R. N. Padhy, Development of antibacterial conjugates using sulfamethoxazole with monocyclic terpenes: a systematic medicinal chemistry based computational approach, *Comput Methods Programs Biomed*, 2017, **140**, 185–194, DOI: 10.1016/j.cmpb.2016.12.013.
20 C. Pigot, D. Brunel, and F. Dumur, *Indane-1,3-Dione: from Synthetic Strategies to Applications*, MDPI, 2022, DOI: 10.3390/molecules27185976.
21 G. P. Yemiş, F. Pagotto, S. Bach and P. Delaquis, Effect of vanillin, ethyl vanillin, and vanillic acid on the growth and heat resistance of cronobacter species, *J. Food Prot.*, 2011, **74**(12), 2062–2069, DOI: 10.4315/0362-028X.JFP-11-230.
22 D. J. Fitzgerald, M. Stratford, M. J. Gasson, J. Ueckert, A. Bos and A. Narbad, Mode of antimicrobial action of vanillin against Escherichia coli, Lactobacillus plantarum and Listeria innocua, *J. Appl. Microbiol.*, 2004, **97**(1), 104–113, DOI: 10.1111/J.1365-2672.2004.02275.X.
23 G. K. Ayyadurai, R. Jayaprakash, A. Shajahan and S. Rathika, Studies on 2-((2, 4-dihydroxybenzylidene) amino)-3-phenylpropanoic acid include antimicrobial, antidiabetic, antioxidant, anticancer, hemolysis, and theoretical QSAR, *J. Biomol. Struct. Dyn.*, 2023, **43**(6), 2864–2876.
24 B. Pizzicato, S. Pacifico, D. Cayuela, G. Mijas and M. Riba-Moliner, Advancements in Sustainable Natural Dyes for Textile Applications: A Review, Multidisciplinary Digital Publishing Institute (MDPI), 2023. DOI: 10.3390/molecules28165954.
25 A. K. Roy Choudhury, Environmental Impacts of the Textile Industry and Its Assessment Through Life Cycle Assessment, in *Roadmap to Sustainable Textiles and Clothing. Textile Science and Clothing Technology*, ed. S. S. Muthu, Springer, Singapore, 2014, ch. 1, pp. 1–39, accessed: Oct. 20, 2025, online, available: DOI: 10.1007/978-981-287-110-7_1.
26 R. Kant, Textile dyeing industry an environmental hazard, *Nat. Sci.*, 2012, **04**(01), 22–26, DOI: 10.4236/ns.2012.41004.
27 S. Sudarshan, *et al.*, *Impact of Textile Dyes on Human Health and Bioremediation of Textile Industry Effluent Using Microorganisms: Current Status and Future Prospects*, Oxford University Press, 2023, DOI: 10.1093/jambio/lxac064.
28 A. P. Periyasamy, *Recent Advances in the Remediation of Textile-Dye-Containing Wastewater: Prioritizing Human Health and Sustainable Wastewater Treatment*, Multidisciplinary Digital Publishing Institute (MDPI), 2024, DOI: 10.3390/su16020495.
29 R. Al-Tohamy, *et al.*, *A Critical Review on the Treatment of Dye-Containing Wastewater: Ecotoxicological and Health Concerns*

of Textile Dyes and Possible Remediation Approaches for Environmental Safety, Academic Press, 2022, DOI: 10.1016/j.ecoenv.2021.113160.

30 S. Suresh, Treatment of Textile Dye Containing Effluents, *Curr. Environ. Eng.*, 2014, **1**(3), 162–184.

31 A. M. S. Jorge, K. K. Athira, M. B. Alves, R. L. Gardas and J. F. B. Pereira, Textile dyes effluents: a current scenario and the use of aqueous biphasic systems for the recovery of dyes, *J. Water Proc. Engineering*, 2023, **55**, 104125, DOI: 10.1016/J.JWPE.2023.104125.

32 S. Dutta, *et al.*, Contamination of textile dyes in aquatic environment: adverse impacts on aquatic ecosystem and human health, and its management using bioremediation, *J. Environ. Manage.*, 2024, **353**, 120103, DOI: 10.1016/J.JENVMAN.2024.120103.

33 P. Dutta, Md. R. Rabbi, M. Abu Sufian and S. Mahjebin, Effects of textile dyeing effluent on the environment and its treatment: a review, *Eng. Appl. Sci. Lett.*, 2022, **5**(1), 1–17, DOI: 10.30538/psrp-easl2022.0080.

34 F. M. Drumond Chequer, G. A. R. de Oliveira, E. R. Anastacio Ferraz, J. Carvalho, M. V. Boldrin Zanoni and D. P. de Oliveir, Textile Dyes: Dyeing Process and Environmental Impact, in *Eco-Friendly Textile Dyeing and Finishing*, InTech, 2013, DOI: 10.5772/53659.

35 R. Atakan, I. Martínez-González, P. Díaz-García and M. Bonet-Aracil, Sustainable Dyeing and Functional Finishing of Cotton Fabric by Rosa canina Extracts, *Sustainability*, 2024, **16**(1), 227, DOI: 10.3390/su16010227.

36 D. A. Yaseen and M. Scholz, Textile dye wastewater characteristics and constituents of synthetic effluents: a critical review, *Center for Environmental and Energy Research and Studies*, 2019, **16**(2), 1193–1226, DOI: 10.1007/s13762-018-2130-z.

37 A. Azanaw, B. Birlie, B. Teshome and M. Jemberie, Textile effluent treatment methods and eco-friendly resolution of textile wastewater, *Case Stud. Chem. Environ. Eng.*, 2022, **6**, 100230, DOI: 10.1016/j.cscee.2022.100230.

38 A. T. Moh Rabti, A. E. Gok, B. Yuzer and H. Selcuk, Evaluation of a sustainable dye-exhausted resin regeneration method for cost-effective decolorization and detoxification of textile wastewater, *Eng. Sci. Technol. Int. J.*, 2025, **63**, 101973, DOI: 10.1016/j.jestch.2025.101973.

39 F. M. Drumond Chequer, G. A. R. de Oliveira, E. R. Anastacio Ferraz, J. Carvalho, M. V. Boldrin Zanoni, and D. P. de Oliveir, Textile Dyes: Dyeing Process and Environmental Impact, in *Eco-Friendly Textile Dyeing and Finishing*, InTech, 2013, DOI: 10.5772/53659.

40 R. Jamee and R. Siddique, Biodegradation of synthetic dyes of textile effluent by microorganisms: an environmentally and economically sustainable approach, *Eur. J. Microbiol. Immunol.*, 2019, **9**(4), 114–118, DOI: 10.1556/1886.2019.00018.

41 E. Khalil, J. Sarkar, Md. M. Rahman, Md. Shamsuzzaman and D. Das, Advanced Technology in Textile Dyeing, in *Advanced Technology in Textiles*, ed. M. Mizanur Rahman, M. Mashud, and M. Mostafizur Rahman, Springer, Singapore, 2023, pp. 97–138, DOI: 10.1007/978-981-99-2142-3_4.

42 K. Ranganathan, K. Karunagaran and D. C. Sharma, Recycling of wastewaters of textile dyeing industries using advanced treatment technology and cost analysis—Case studies, *Resour., Conserv. Recycl.*, 2007, **50**(3), 306–318, DOI: 10.1016/J.RESCONREC.2006.06.004.

43 A. Arumugam, V. R. Babu, S. Sundaresan and T. Durai, *Sustainable dyeing techniques: advancements and innovations in the textile industry*, 2021, available: https://www.researchgate.net/publication/378260407.

44 F. Kane, J. Shen, L. Morgan, C. Prajapati, J. Tyrer and E. Smith, *Innovative Technologies for Sustainable Textile Coloration, Patterning, and Surface Effects*, ed. S. S. Muthu and M. A. Gardetti, Springer, Cham, 2020, pp. 99–127, DOI: 10.1007/978-3-030-38545-3_4.

45 C. Stone, F. M. Windsor, M. Munday and I. Durance, Natural or synthetic – how global trends in textile usage threaten freshwater environments, *Sci. Total Environ.*, 2020, **718**, 134689, DOI: 10.1016/j.scitotenv.2019.134689.

46 E. Ozturk, H. Koseoglu, M. Karaboyaci, N. O. Yigit, U. Yetis and M. Kitis, Sustainable textile production: cleaner production assessment/eco-efficiency analysis study in a textile mill, *J. Cleaner Prod.*, 2016, **138**, 248–263, DOI: 10.1016/J.JCLEPRO.2016.02.071.

47 Y. Gai, Y. Qiao, H. Deng and Y. Wang, Investigating the eco-efficiency of China's textile industry based on a firm-level analysis, *Sci. Total Environ.*, 2022, **833**, 155075, DOI: 10.1016/J.SCITOTENV.2022.155075.

48 B. J. Singh, A. Chakraborty and R. Sehgal, *A Systematic Review of Industrial Wastewater Management: Evaluating Challenges and Enablers*, Academic Press, 2023, DOI: 10.1016/j.jenvman.2023.119230.

49 K. Gomes, S. Caucci, J. Morris, E. Guenther and J. Miggelbrink, Sustainability transformation in the textile industry—The case of wastewater management, *Business Strategy and Development*, 2024, **7**(1), e324, DOI: 10.1002/bsd2.324.

50 L. Siliņa, I. Dāboliņa and E. Lapkovska, *Sustainable Textile Industry – Wishful Thinking or the New Norm: A Review*, SAGE Publications Ltd, DOI: 10.1177/15589250231220359, 2024.

51 K. Yılmaz, İ. Ö. Aksu, M. Göçken and T. Demirdelen, Sustainable Textile Manufacturing with Revolutionizing Textile Dyeing: Deep Learning-Based, for Energy Efficiency and Environmental-Impact Reduction, Pioneering Green Practices for a Sustainable Future, *Sustainability*, 2024, **16**(18), 8152, DOI: 10.3390/su16188152.

52 A. Hasanbeigi and L. Price, A technical review of emerging technologies for energy and water efficiency and pollution reduction in the textile industry, *J. Cleaner Prod.*, 2015, **95**, 30–44, DOI: 10.1016/J.JCLEPRO.2015.02.079.

53 N. S. Elshemy, Unconventional Natural Dyeing Using Microwave Heating with Cochineal as Natural Dyes, *Res. J. Text. Apparel*, 2011, **15**(4), 26–36, DOI: 10.1108/RJTA-15-04-2011-B004.

54 A. L. Mohamed, S. Shaarawy, N. S. El-Shiemy, A. Hebiesh and A. G. Hassabo, Treatment of Cotton Fabrics using Polyamines for Improved Coloration with Natural Dyes Extracted from Plant and Insect Sources, *Egypt. J. Chem.*, 2023, **66**(3), 1–19, DOI: 10.21608/EJCHEM.2022.137464.6053.

55 J.-O. Kim, M. K. Traore and C. Warfield, The Textile and Apparel Industry in Developing Countries, *Text. Prog.*, 2006, **38**(3), 1–64, DOI: 10.1533/tepr.2006.0003.

56 J. Malaga and S. Mohanty, The Agreement on Textiles and Clothing: Is It a WTO Failure?, *The Estey Centre Journal of International Law and Trade Policy*, 2003, **4**, 75–85.

57 C. Palm, S. E. Cornell and T. Häyhä, Making Resilient Decisions for Sustainable Circularity of Fashion, *Circ. Econ. Sustainability*, 2021, **1**(2), 651–670, DOI: 10.1007/s43615-021-00040-1.

58 B. Harsanto, J. I. Farras, and D. Indradi, Sustainability Innovation in the Textile Industry, in *Industry and Innovation: Textile Industry*, ed. J. M. Martins, Springer, Cham, 2024, pp. 339–358, DOI: 10.1016/C2020-0-03246-9.

59 B. Harsanto, I. Primiana, V. Sarasi and Y. Satyakti, *Sustainability Innovation in the Textile Industry: A Systematic Review*, MDPI, 2023, DOI: 10.3390/su15021549.

60 L. Lara, I. Cabral and J. Cunha, *Ecological Approaches to Textile Dyeing: A Review*, MDPI, 2022, DOI: 10.3390/su14148353.

61 S. Nain, R. Singh and S. Ravichandran, *Importance of Microwave Heating in Organic Synthesis*, 2019, [online], available: http://ajchem-a.comhttp://ajchem-a.com.

62 M. J. Collins, *Future trends in microwave synthesis, Future Medicinal Chemistry*, 2010, **2**(2), 151–155, DOI: 10.4155/fmc.09.133.

63 J. L. Krstenansky and I. Cotterill, Recent advances in microwave-assisted organic syntheses., *Curr. Opin. Drug Discov. Devel.*, 2000, **3**(4), 454–461, DOI: 10.1002/chin.200049266.

64 F. E. Hanna and C. A. Hunter, Polarisation effects on the H-bond acceptor properties of sulfonamides, *Chem. Commun.*, 2024, **60**(82), 11750–11753, DOI: 10.1039/d4cc03530e.

65 M. Megally, N. S. Elshemy, K. Haggag and A. I. Hashem, Development and Optimization of A Non-traditional Extraction Process of Yellow Colorant from Safflower Petals as A Natural Colorant, *Egypt. J. Chem.*, 2019, **62**(2), 231–246, DOI: 10.21608/EJCHEM.2018.5119.1453.

66 K. Haggag, N. S. Elshemy and W. Niazy, Recycling of Waste PET into Useful Alkyd Resin Synthesis by Microwave Irradiation and Applied in Textile Printing, *Res. J. Text. Apparel*, 2014, **18**(1), 80–88, DOI: 10.1108/RJTA-18-01-2014-B010.

67 N. Sobh, N. S. Elshemy, S. Nassar and M. Ali, New insights into the role of color extraction from (*Aegle marmelos* leaf) using a non-traditional heating source, *Pigm. Resin Technol.*, 2025, **54**(1), 53–64, DOI: 10.1108/PRT-05-2023-0041.

68 N. S. Elshemy, Unconventional Natural Dyeing Using Microwave Heating with Cochineal as Natural Dyes, *Res. J. Text. Apparel*, 2011, **15**(4), 26–36, DOI: 10.1108/RJTA-15-04-2011-B004.

69 N. S. Elshemy, M. H. Elshakankery, S. M. Shahien, K. Haggag and H. El-Sayed, Kinetic investigations on dyeing of different polyester fabrics using microwave irradiation, *Egypt. J. Chem.*, 2017, **60**, 79–88, DOI: 10.21608/ejchem.2017.1604.1131.

70 O. Allam, N. S. Elshemy and H. El-Sayed, Simple and Easily Applicable Method for Reducing Freshwater Consumption in Dyeing of Wool Fabric, *J. Nat. Fibers*, 2022, **19**(3), 895–904, DOI: 10.1080/15440478.2020.1764439.

71 N. S. El-Shemy and N. S. El-Hawary, Basic and Reactive-Dyeable Polyester Fabrics Using Lipase Enzymes, *J. Chem. Eng. Process Technol.*, 2016, **07**(01), 271, DOI: 10.4172/2157-7048.1000271.

72 Chemical Computing Group Inc. Molecular operating environment (MOE) 2016.1010, online, available: https://www.chemcomp.com/en/index.htm.

73 E. A. E. El-Helw, A. Y. Alzahrani and S. K. Ramadan, Synthesis and antimicrobial activity of thiophene-based heterocycles derived from thiophene-2-carbohydrazide, *Future Med. Chem.*, 2024, **16**(5), 439–451.

74 H. M. Helmy, M. M. Kamel, K. Hagag, N. El-Hawary and N. S. El-Shemy, Antimicrobial activity of dyed wool fabrics with peanut red skin extract using different heating techniques, *Egypt. J. Chem.*, 2017, **60**, 103–116, DOI: 10.21608/ejchem.2017.1601.1129.

75 N. F. Ali and R. S. R. El-Mohamedy, Eco-friendly and protective natural dye from red prickly pear (*Opuntia lasiacantha* Pfeiffer) plant, *J. Saudi Chem. Soc.*, 2011, **15**(3), 257–261, DOI: 10.1016/j.jscs.2010.10.001.

76 J. Mai, T. Lu, P. Xu, Z. Lian, M. Li and W. Lu, Predicting the maximum absorption wavelength of azo dyes using an interpretable machine learning strategy, *Dyes Pigm.*, 2022, **206**, 110647, DOI: 10.1016/j.dyepig.2022.110647.

77 R. Diana, *et al.*, Experimental and Theoretical Insights into a Novel Lightfast Thiophene Azo Dye, *Crystals*, 2024, **14**(1), 31, DOI: 10.3390/cryst14010031.

78 A. Z. Omar, *et al.*, Ultrasonic versus dispersing agent dyeing process of polyester fabrics using novel chalcone azo naphthol and hydroxyquinoline-based disperse dyes: synthesis, characterization, and computational analysis, *J. Mol. Liq.*, 2025, **426**, 127456, DOI: 10.1016/J.MOLLIQ.2025.127456.

79 M. Rehan, H. El-Sayed, N. S. El-Hawary, H. Mashaly and N. S. Elshemy, Chemically Modified Extract of Peanut Red Skin: Toward Functional Dyeing of Textile Fabrics and Study Adsorption Kinetics and Adsorption Isotherm of Dyeing Process, *Ind. Eng. Chem. Res.*, 2024, **63**(26), 11301–11319, DOI: 10.1021/acs.iecr.4c01969.

80 A. E. Morgan, J. E. Salcedo-Sora and M. T. Mc Auley, A new mathematical model of folate homeostasis in *E. coli* highlights the potential importance of the folinic acid futile cycle in cell growth, *BioSystems*, 2024, **235**, 105088, DOI: 10.1016/j.biosystems.2023.105088.

81 O. Sköld, Sulfonamide resistance: mechanisms and trends, *Drug Resistance Updates*, 2000, **3**(3), 155–160, DOI: 10.1054/drup.2000.0146.

82 S. Ebara, H. Naitio, K. Nakazawa, F. Ishii and M. Nakamura, FTR1335 Is a Novel Synthetic Inhibitor of *Candida albicans* *N*-Myristoyltransferase with Fungicidal Activity, *Biol. Pharm. Bull.*, 2005, **28**(4), 591–595.

83 Y. Zhao, *et al.*, Pterin–sulfa conjugates as dihydropteroate synthase inhibitors and antibacterial agents, *Bioorg. Med. Chem. Lett.*, 2016, **26**(16), 3950–3954, DOI: 10.1016/j.bmcl.2016.07.006.

84 S. Sogabe *et al.*, Crystal Structures of Candida albicans N-Myristoyltransferase with Two Distinct Inhibitors membranes and that facilitates interactions with hydrophobic protein domains [6, 7], *Nmt Participates in Diverse Biological Processes, Including Signal Transduc*, 2002.

85 J. T. Ortega, M. L. Serrano, F. H. Pujol and H. R. Rangel, Unrevealing sequence and structural features of novel coronavirus using *in silico* approaches: the main protease as molecular target, *EXCLI J.*, 2020, **19**, 400–409, DOI: 10.17179/excli2020-1189.

86 E. El-Sayed Ebead, A. Aboelnaga, E. Nassar, M. M. Naguib and M. F. Ismail, Ultrasonic-induced synthesis of novel diverse arylidenes via Knoevenagel condensation reaction. Antitumor, QSAR, docking and DFT assessment, *RSC Adv.*, 2023, **13**(42), 29749–29767, DOI: 10.1039/d3ra05799b.

87 A. Aboelnaga, S. Soror, E. Nassar, S. Elabbady and A. M. Fahim, Novel bis pyrimidine-pyrazolone and pyridinyl-4,5-dihydropyrimido[2,1[1]-c,1,2,4]triazepine utilized ultrasonic energy, anti-proliferative activity, docking simulation, and theoretical investigation, *J. Mol. Struct.*, 2023, **1294**, 136517, DOI: 10.1016/j.molstruc.2023.136517.

88 F. S. Alamro, H. A. Ahmed, S. A. Popoola and A. Aboelnaga, Synthesis, phase behavior and computational simulations of a pyridyl-based liquid crystal system, *Molecules*, 2021, **26**(21), 6416, DOI: 10.3390/molecules26216416.

89 M. F. Ismail, A. Aboelnaga, M. M. Naguib and H. M. Ismaeel, Synthesis, Anti-Proliferative Activity, DFT and Docking Studies of Some Novel Chloroquinoline-Based Heterocycles, *Polycyclic Aromat. Compd.*, 2023, **44**(9), 5951–5982.

90 C. Liu, *et al.*, *Computational Network Biology: Data, Models, and Applications*, Elsevier B.V., 2020, DOI: 10.1016/j.physrep.2019.12.004.

91 F. Wohlrab, A. Jamieson, R. Mengel and W. Guschlbauer, The effect of 2′-fluoro-2′-deoxycytidine on herpes virus growth, *Biochim. Biophys. Acta*, 1985, **824**(3), 233–242, DOI: 10.1016/0167-4781(85)90053-3.

92 P. Glue, The clinical pharmacology of ribavirin, *Semin. Liver Dis.*, 1999, **19**(1), 17–24.

93 S. Yamamoto, *et al.*, Proposal of potent inhibitors for a bacterial cell division protein ftsz: molecular simulations based on molecular docking and *ab initio* molecular orbital calculations, *Antibiotics*, 2020, **9**(12), 1–15, DOI: 10.3390/antibiotics9120846.

94 S. Xavier, S. Periandy and S. Ramalingam, NBO, conformational, NLO, HOMO–LUMO, NMR and electronic spectral study on 1-phenyl-1-propanol by quantum computational methods, *Spectrochim. Acta, Part A*, 2015, **137**, 306–320, DOI: 10.1016/j.saa.2014.08.039.

95 A. G. Ibrahim, W. E. Elgammal, E. El-Sayed Ebead, M. F. Ismail, M. H. Sharaf and A. Aboelnaga, Functionalized chitosan with new acrylohydrazide derivative: synthesis, characterization, DFT calculations, antimicrobial and antiproliferative activities, *J. Mol. Struct.*, 2025, **1341**, 142607, DOI: 10.1016/j.molstruc.2025.142607.

96 L. Zhang, C. Li and S. Pang, *Dual-aromaticity in Nitrogen-Rich Compounds: from Fundamental Concepts to the Application of High-Energy-Density Materials*, Elsevier B.V., DOI: 10.1016/j.ccr.2025.217081, 2026.

97 D. Shin and Y. J. Jung, Molecular electrostatic potential as a general and versatile indicator for electronic substituent effects: statistical analysis and applications, *Phys. Chem. Chem. Phys.*, 2022, **24**(42), 25740–25752, DOI: 10.1039/d2cp03244a.